



**HAL**  
open science

## **Biomass steam gasification kinetics: relative impact of char physical properties vs. inorganic composition**

Tilia Dahou, Françoise Defoort, Hong Nam Nguyen, Simona Bennici, Mejdi Jeguirim, Capucine Dupont

► **To cite this version:**

Tilia Dahou, Françoise Defoort, Hong Nam Nguyen, Simona Bennici, Mejdi Jeguirim, et al.. Biomass steam gasification kinetics: relative impact of char physical properties vs. inorganic composition. Biomass Conversion and Biorefinery, 2022, 12, pp.3475-3490. 10.1007/s13399-020-00894-9 . hal-02958145

**HAL Id: hal-02958145**

**<https://hal.science/hal-02958145>**

Submitted on 16 Nov 2020

**HAL** is a multi-disciplinary open access archive for the deposit and dissemination of scientific research documents, whether they are published or not. The documents may come from teaching and research institutions in France or abroad, or from public or private research centers.

L'archive ouverte pluridisciplinaire **HAL**, est destinée au dépôt et à la diffusion de documents scientifiques de niveau recherche, publiés ou non, émanant des établissements d'enseignement et de recherche français ou étrangers, des laboratoires publics ou privés.

# Biomass steam gasification kinetics: relative impact of char physical properties vs. inorganic composition

Tilia DAHOU<sup>a,b,c,d</sup>, Françoise DEFOORT<sup>a\*</sup>, Hong Nam NGUYEN<sup>e</sup>, Simona BENNICI<sup>b,c</sup>, Mejdi JEGUIRIM<sup>b,c</sup>,  
Capucine DUPONT<sup>f</sup>

<sup>a</sup>Université Grenoble Alpes, CEA, LITEN, DTBH, 17 avenue des Martyrs, 38054 Grenoble CEDEX 09,  
France

<sup>b</sup>Université de Haute-alsace, CNRS, IS2M UMR 7361, F-68100 Mulhouse, France

<sup>c</sup>Université de Strasbourg, France

<sup>d</sup>Agence de l'Environnement et de la Maîtrise de l'Energie (ADEME), 20 avenue du Grésillé, BP 90406,  
49004 Angers CEDEX 01, France

<sup>e</sup>Energy University of Science and Technology of Hanoi (USTH), Vietnam Academy of Science and  
Technology, Hanoi, Vietnam

<sup>f</sup>IHE Delft Institute for Water Education, Westvest 7, 2611 AX Delft, The Netherlands

\*Corresponding author: francoise.defoort@cea.fr

## Highlights

- Steam gasification chars were characterized at several conversion values
- Both char physical properties and inorganic composition were evaluated
- Inorganic composition is the main parameter explaining the gasification kinetics
- Some char physical properties depend on the inorganic composition

## Abstract

During biomass gasification, both the char physical properties and the biomass inorganic composition are known to have a significant influence the reaction kinetics. However, the impact of the inorganic content seems more pronounced than that of the char features, even if no clear explanations has been found, yet. With the aim to clarify this point, two biomass species with significant difference in the inorganic compositions were gasified under steam and the char (solid residue) obtained at various gasification conversion values were characterized. Both the char physico-chemical properties (chemical composition, carbon structure, porosity and surface chemistry) and the gasification kinetic behavior were then investigated. Regarding the inorganic composition, both the elemental composition and the inorganic compounds nature were obtained. Experimental results were compared to simulation results at thermodynamic equilibrium obtained with the FactSage 7.2 software. The results showed that the physical properties of the carbon matrix do not have a strong influence on the gasification reactivity. On the opposite, the inorganic composition is the main parameter that seems to explain the differences between the gasification kinetic behavior of the two investigated chars (obtained starting from two different biomass sources). Moreover, the presence of

inorganics also seems to affect the physical properties of the chars, namely the microporosity and the amount of surface functions.

## Keywords

steam gasification; reaction kinetics; inorganic compounds; char physical properties

## 1. Introduction

In the context of climate change, biomass gasification is a promising thermochemical conversion process for bioenergy production. It converts lignocellulosic biomass into a syngas, i.e. a mixture of mainly CO and H<sub>2</sub>, which can be further processed to obtain heat and power or gaseous and liquid fuels.

The knowledge of the gasification reaction kinetics is essential to the design of the industrial reactors. Whatever the gasifier type, the kinetics of the reactions must be known and controlled as well as the mass and heat transfers. This can be easily understood in the case of the dual fluidized bed reactor. It consists in two distinct fluidized beds. In one, biomass is gasified with the gasifying agent. In the other, the combustion of the residual char from gasification occurs in air or O<sub>2</sub>. Those two parts are joined in a loop, with the bed material circulating between the two reactors. In this case, the gasification kinetics need to be controlled so that enough char goes to the combustion side to produce the heat necessary to the process.

Several parameters influence the gasification kinetics: environmental parameters and biomass-related parameters.

Environmental parameters are related to the atmosphere and temperature. Biomass gasification can be carried out using different gasifying environments. Air, oxygen, steam, carbon dioxide and combinations of these gases can be used as gasifying agents. At equal oxygen content in the gas flow, steam gasification is faster than CO<sub>2</sub> gasification. For example, in their study on woodchip char at 900 °C, Ahmed et al. (Ahmed and Gupta, 2011) observed that the use of steam instead of CO<sub>2</sub> divided the gasification time by almost three and increased the gasification rate by a factor of almost two. For both gasifying agents, the reaction rate increases with the steam or CO<sub>2</sub> partial pressure increase (Marquez-Montesinos et al., 2002). In the same way, the reaction rate increases when the gasification temperature increases (Marquez-Montesinos et al., 2002).

The two main biomass-related parameters mentioned in literature are the morphological structure of the char and its composition in inorganic matter (Di Blasi, 2009). As synthesized in Di Blasi's review (Di Blasi, 2009), the morphological structure is particularly influenced by the release of the volatile species during the pyrolysis, which is controlled by the operating conditions of this step. It has been shown that high heating rate pyrolysis produces a char that is more reactive in gasification than low heating rate pyrolysis. Chars from low heating rate pyrolysis keep their natural porosity, while chars from high heating rate pyrolysis form larger cavities (Di Blasi, 2009; Septien et al., 2018). This larger surface area in the case of high heating rate pyrolysis along with the higher content in O and H results in more available active sites (Guerrero et al., 2008). Regarding inorganic content, some inherent inorganic elements are known to have a significant influence on char gasification kinetics. In particular, it has been shown that alkali and alkaline earth metals (AAEMs) tend to have a catalytic effect that enhances biomass gasification kinetics (Di Blasi, 2009). More specifically, alkali metals, and in particular K, which is more present in biomass than Na, are reported to be more active than alkaline earth metals. No significant effect was observed for Mg in the literature (Zahara et al., 2018; Zhang et al., 2008). The catalytic activity of AAEMs was reported to be, in decreasing order, K, Na, Ca

and Mg (Huang et al., 2009; Yip et al., 2010; Zhang et al., 2008). Other elements present in the biomass can have the opposite effect and slow the gasification down. In particular, Al, Si and P have been reported to inhibit the gasification (Arnold and Hill, 2019; Bouraoui et al., 2016; Dupont et al., 2016; Link et al., 2010; Zhang et al., 2008). In the case of lignocellulosic biomass, Al and P are usually found in low amounts whereas Si can reach high concentrations.

It seems that, for similar conditions for the production of the char, the influence of the morphological structure is weaker than the influence of the inorganic composition, though no clear conclusion is given in literature (Di Blasi, 2009; Gupta et al., 2018).

Based on the literature just summarized, the objective of this work was to analyze the relative influence of the inorganic elements compared to that of the physical properties of biomass-derived chars on the gasification kinetics. In order to bring more insights to the existing literature, various chars obtained from two different biomass presenting a significant difference in their inorganic compositions were characterized after steam gasification at variable conversion values. Both the char physico-chemical properties and the kinetic behavior were taken into account.

## 2. Materials and experimental installations

### 2.1. List of biomass species

Two biomass samples, agricultural residues, were selected for this study. Samples were ground below 200  $\mu\text{m}$  in a Pulverisette 14 rotor mill (FRITSCH, Idar-Oberstein, Germany). The ash content and inorganic element composition of the samples were measured according to solid fuel standards NF EN 14775 (European Standards, 2009) and NF EN ISO 16967 (International Organization for Standardization, 2015), respectively. The obtained values for each biomass sample are presented in Table 1. From these values, the three major inorganic elements in each sample were identified.

Table 1 | Ash content, elemental composition and gasification average reactivity of the biomass samples (in dry basis).

Property	Unit	Rice husks	Sunflower seed shells
Ash at 550 °C	wt%	14.1	3.3
C	wt%	41.6	50.2
H	wt%	5.2	6.5
O*	wt%	45.1	40.6
N	wt%	0.5	0.7
S	wt%	0.1	0.1
Cl	wt%	0.1	0.1
Si	mg.kg <sup>-1</sup>	63955	194
K	mg.kg <sup>-1</sup>	5822	9729
Ca	mg.kg <sup>-1</sup>	1797	4489
Mg	mg.kg <sup>-1</sup>	659	1838
P	mg.kg <sup>-1</sup>	981	896
Na	mg.kg <sup>-1</sup>	413	9
Al	mg.kg <sup>-1</sup>	228	150
Fe	mg.kg <sup>-1</sup>	192	1099
Mn	mg.kg <sup>-1</sup>	195	23
SiO <sub>2</sub>	wt% in ashes	97.2	1.3
K <sub>2</sub> O	wt% in ashes	5.0	35.5
CaO	wt% in ashes	1.8	19.0
MgO	wt% in ashes	0.8	9.2
P <sub>2</sub> O <sub>5</sub>	wt% in ashes	1.6	6.2
Na <sub>2</sub> O	wt% in ashes	0.4	0.0
Al <sub>2</sub> O <sub>3</sub>	wt% in ashes	0.3	0.9
Fe <sub>2</sub> O <sub>3</sub>	wt% in ashes	0.2	4.8
MnO	wt% in ashes	0.2	0.1
Main Inorganic Elements	—	Si – K – Ca	K – Ca – Mg
Gasification average reactivity between 1 and 80% conversion	%.min <sup>-1</sup>	1.4	30.3

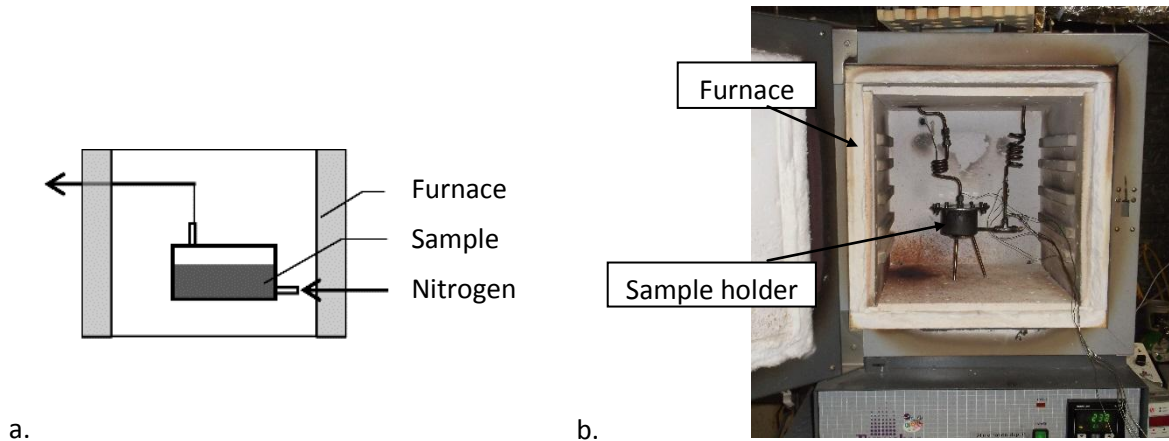
\*Total (i.e. organic and inorganic) oxygen calculated by difference with all other elements.

## 2.2. Experimental set-ups

### 2.2.1. Pyrolysis furnace

Chars were produced in large quantities, i.e. several grams, in the pyrolysis installation illustrated in Figure 1.

It consists of a stainless steel sample holder of 40 mm height and 70 mm diameter swept by  $1 \text{ L}\cdot\text{min}^{-1}$   $\text{N}_2$  and placed in a furnace.



a. b.  
Figure 1 | Pyrolysis furnace a. scheme and b. picture.

Low heating rate (LHR) pyrolysis of the biomass samples was carried out. The sample holder was filled in with 30 to 50 g of ground sample depending on the biomass. Biomass samples were then heated to  $450 \text{ }^\circ\text{C}$  at a heating rate of  $10 \text{ }^\circ\text{C}\cdot\text{min}^{-1}$  and kept at this temperature for 60 min.

The mass of sample was weighted before and after pyrolysis to determine the char yield.

The obtained char samples are referred to as RHB\_charM and SFS\_charM for rice husks and sunflower seed shells, respectively.

### 2.2.2. Thermogravimetric analyzer

Thermogravimetric analysis (TGA) was used to determine the intrinsic kinetic behavior of the samples—raw biomass or char. Experiments were carried out at atmospheric pressure using a Setsys thermobalance (SETARAM, Caluire, France) coupled with a Wetsys steam generator described elsewhere (Dupont et al., 2011).

The experimental procedure was slightly different for raw biomass and for char, so that in both cases the pyrolysis and gasification steps were separated (Figure 2).

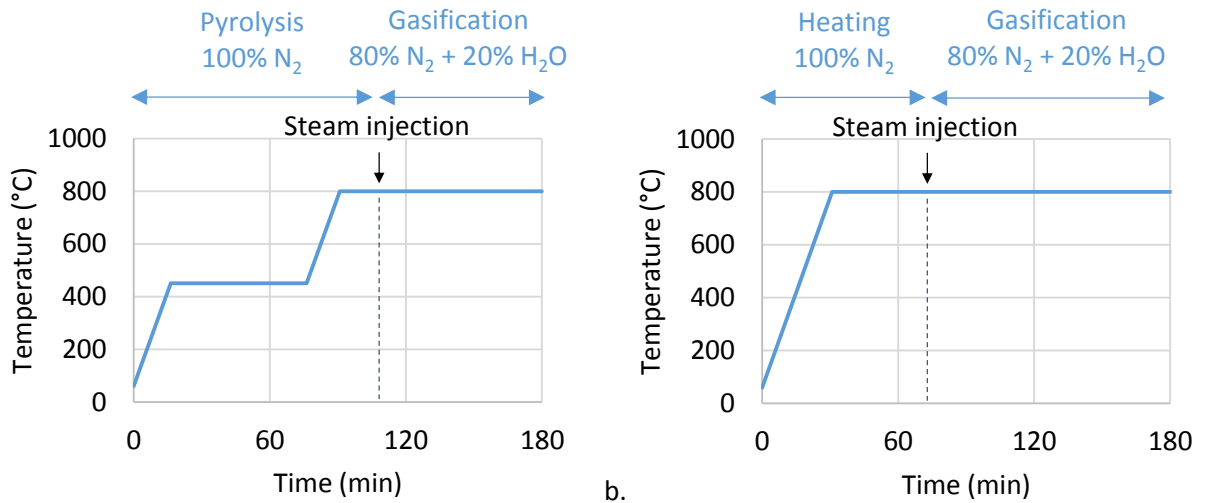


Figure 2 | TGA procedure for a. raw biomass and b. char.

In the case of raw biomass (Figure 2a), the procedure described by Hognon *et al.* (Hognon *et al.*, 2014) was applied to a mass of approximately 15 mg to be in chemical regime (Dupont *et al.*, 2011).

In the case of char (Figure 2b), the holding time at 450 °C was not necessary as pyrolysis had already been conducted. The procedure described by Dupont *et al.* (Dupont *et al.*, 2016) was applied to a mass of approximately 4 mg to be in chemical regime (Dupont *et al.*, 2011).

All experiments were conducted at least in duplicates. Only one of the repetitions was selected to be plotted as curve.

### 2.2.3. Macro-thermogravimetric reactor

The macro-thermogravimetric reactor (macroTG) is illustrated in Figure 3. It has been described by Nguyen *et al.* (Nguyen *et al.*, 2018).

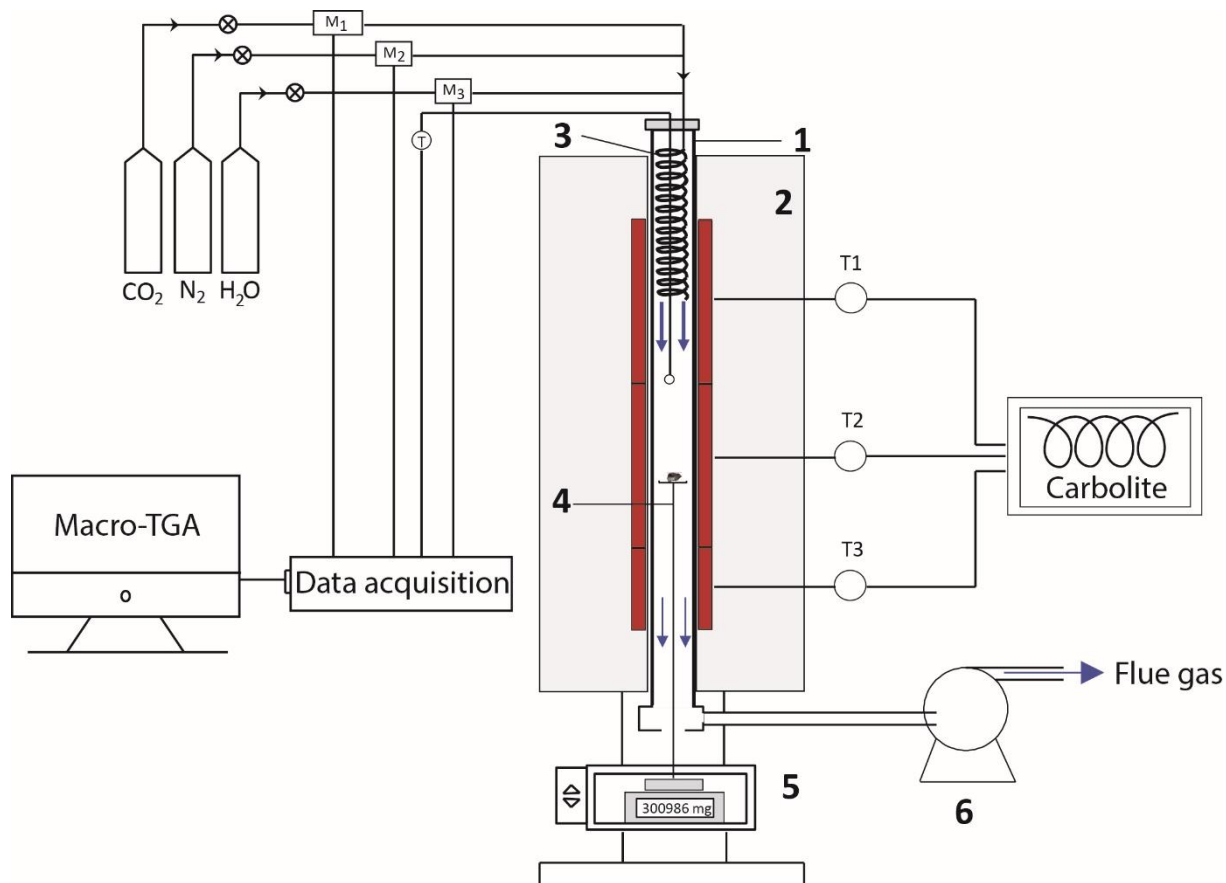


Figure 3 | Macro-thermogravimetric reactor.

Steam gasification experiments were carried out under fixed operating conditions. For each experiment, the reactor was first heated to 800°C. When the desired temperature was reached, approximately 150 mg of char sample was lifted to the desired position inside the reactor. The sample mass was selected to be in the chemical regime. It was initially placed under inert atmosphere at an N<sub>2</sub> flow of 5 NL.min<sup>-1</sup> to remove all residual volatiles and moisture adsorbed during storage.

When a constant mass was reached, the gas flow was switched to a mixture of 20 vol% H<sub>2</sub>O in N<sub>2</sub> to conduct the gasification. Chars were collected at conversion values of X = 0%, 25%, 50%, 75% and 100%. When the needed conversion time (which was predetermined) was reached, the gas flow was switched to 100% N<sub>2</sub> again until the complete cool down of the char.

The list of samples is summarized in Table 2.

Table 2 | List of samples obtained from pyrolysis and gasification of rice husks and sunflower seed shells

Sample production conditions	Rice husks	Sunflower seed shells
Char from pyrolysis at 450 °C	RHB_charM	SFS_charM
Char from pyrolysis at 800 °C, i.e. X = 0%	RHB_X0	SFS_X0
Char from gasification at 800 °C stopped at X = 25%	RHB_X25	SFS_X25
Char from gasification at 800 °C stopped at X = 50%	RHB_X50	SFS_X50
Char from gasification at 800 °C stopped at X = 75%	RHB_X75	SFS_X75
Ashes from gasification at 800 °C, i.e. X = 100%	RHB_X100	SFS_X100

#### 2.2.4. Data treatment

For both the TGA and the macroTG, gasification solid conversion was defined from the mass loss measured as a function of time by using the following expression:

$$X(t) = \frac{m_{i\text{char}} - m(t)}{m_{i\text{char}} - m_f}, \quad (1)$$

where  $m_{i\text{char}}$  is the mass of char before gasification (at the time of steam injection).

The gasification rate was then defined as the variation of conversion versus time:

$$r(t) = \frac{dX}{dt}. \quad (2)$$

An average reactivity between two values of conversion  $X_1$  and  $X_2$  was also defined:

$$r_{X_1-X_2} = \frac{\int_{t_{X_1}}^{t_{X_2}} \frac{r(t)dt}{1-X(t)}}{t_{X_2} - t_{X_1}}. \quad (3)$$

There is no standardized definition for the reactivity (Barrio et al., 2001). In this study, the average reactivity was calculated between 1 and 80% conversion as in several investigations in literature (Barrio et al., 2001; Dupont et al., 2011; Hognon et al., 2014). This choice allowed to obtain a trend that was not affected by the particular phenomena that can occur at high conversion values.

### 2.3. Characterization techniques

Characterization techniques usually used for chars were applied. These techniques mainly focus on the carbonaceous matrix which generally represents 99% of the char mass in the case of woods. However, agricultural residues have a higher ash content—up to 14.1 wt% in the present study (Table 1)—which then could not be neglected. Therefore, the determination of the inorganic compounds contained in the chars was also performed. In particular, Raman spectroscopy, which is traditionally used to characterize carbon structure, was also used here to identify mineral phases in the chars.

The characterization techniques and the corresponding evaluated properties are listed in Table 3.

Table 3 | Characterization techniques and the properties they measure.

Characterization technique	Measured property
Raman spectroscopy	Structure of the carbon matrix
N <sub>2</sub> and CO <sub>2</sub> adsorption	Porosity of the carbon matrix
TPD–MS	Surface chemistry of the carbon matrix
ICP–AES	Inorganic elemental composition
SEM–EDX	Morphology of the chars and surface elemental composition
P–XRD	Crystalline phases

### 2.3.1. Raman spectroscopy

Raman spectroscopy was used to study the structure of the char carbon matrix. Acquisition of the Raman spectra was performed with a BX40 LabRam, Jobin Yvon Horiba spectrometer in a backscattered configuration with a laser at 532 nm. For each sample a layer of the material was placed on a glass slide and Raman spectra was recorded at 9 locations.

The Raman spectra were analyzed as a combination of five bands corresponding to five carbonaceous structures (Chabalala et al., 2011; Guizani et al., 2016; Liu et al., 2015; Sadezky et al., 2005; Sheng, 2007):

- The G band at 1590 cm<sup>-1</sup> is the only existing band for perfect graphite. It corresponds to the stretching vibration mode with E<sub>2g</sub> symmetry in the aromatic layers of the graphite crystallite.
- The D1 band at 1350 cm<sup>-1</sup> is related to graphene layers edges. It corresponds to graphitic lattice vibration mode with A<sub>1g</sub> symmetry and in-plane imperfections such as defects and hetero-atoms.
- The D2 band at 1620 cm<sup>-1</sup> is related to surface graphene layers. It corresponds to the stretching vibration mode with E<sub>2g</sub> symmetry in the graphene layers which are not directly sandwiched between two other graphene layers.
- The D3 band at 1500 cm<sup>-1</sup> is found in poorly organized materials. It corresponds to sp<sup>2</sup> carbons in amorphous structures (organic molecules, fragments, functional groups). It is suggested as being related to reactive sites.
- The D4 band at 1200 cm<sup>-1</sup> is found in very poorly organized materials. It corresponds to sp<sup>2</sup>-sp<sup>3</sup> sites at the periphery of crystallites and to C–C and C=C stretching vibrations of polyene-like structures. It is suggested as being related to reactive sites.

Band fitting was carried out with the Origin software from OriginLab. Band intensity ratios were calculated with the intensity of each taken as the fitted area of the peak. Ratios of ID1/IG, ID2/IG, ID3/IG, ID4/IG, IG/IALL and ID3/IALL were calculated with ID1, ID2, ID3, ID4, IG and IALL the intensity of the bands D1, D2, D3, D4, G and the sum of the intensities of all bands respectively.

In the Raman shift range of the spectra acquisition, peaks corresponding to some inorganic compounds could be recorded in addition to the carbon matrix bands. These peaks were identified by comparison to spectra from the Handbook of Minerals Raman Spectra (ENS Lyon, 2019).

### 2.3.2. N<sub>2</sub> and CO<sub>2</sub> adsorption

N<sub>2</sub> adsorption and CO<sub>2</sub> adsorption were used to characterize the porosity of the carbon matrix of the chars. The samples were outgassed overnight at 300 °C before the analyses. N<sub>2</sub> adsorption was

conducted with a Micrometrics ASAP 2024 instrument at -198°C. CO<sub>2</sub> adsorption was conducted with a Micrometrics ASAP 2020 instrument at 0 °C. For both adsorbable molecules, pore size distribution was determined with the DFT model for slit pores with a finite depth. The porosity of the inorganic fraction of the chars was neglected. The results were then expressed in dry ash-free basis.

### 2.3.3. Temperature programmed desorption coupled to mass spectrometry

Temperature programmed desorption coupled to mass spectrometry (TPD–MS) was used to analyze the surface chemistry of the char carbon matrix. Approximately 10 mg of sample were placed in a quartz crucible. This crucible was introduced in a heated quartz tubular reactor connected to a vacuum pump and a mass spectrometer. The analysis consisted in two steps. First, the sample was outgassed by creating vacuum at ambient temperature. Then, the sample was heated to 800 °C at a rate of 5 °C/min and kept at this temperature for 30 min. The emitted gas CO<sub>2</sub>, CO, H<sub>2</sub>, H<sub>2</sub>O, CH<sub>4</sub> and SO<sub>2</sub> were continuously quantified by mass spectrometry. The total pressure was also measured with a Bayard Alpert gauge. Mass balance was checked from these two measurements. For each gas, desorption was calculated by integrating the TPD–MS curves. The results were expressed in dry ash-free basis.

### 2.3.4. Inductively coupled plasma with atomic emission spectroscopy

Inductively coupled plasma with atomic emission spectroscopy (ICP–AES) was used to measure the inorganic elemental composition of the chars. The analysis was conducted after mineralization of the samples for all inorganic species, except for silicon which underwent an alkaline melting. The measured elements were: Si, K, Ca, Mg, P, Na, Al and Fe. Measures could not be conducted on samples SFS\_X50, both X75 and both X100 because of low quantities obtained after gasification tests. For samples X25 and X50, Na, Al and Fe were not measured.

Results are given as mass fractions  $C_i^{raw}$  or  $C_i^{char}$  for raw biomass or char, respectively. It corresponds to the mass of element in the sample divided by the mass of sample—the sample being either raw biomass or char.

These mass fractions were used to calculate the volatilization yield  $V_i^{char}$  of each element *i* by comparison with the raw biomass content. It was defined as follows:

$$V_i^{char} = \frac{C_i^{raw} - C_i^{char} \times \text{char yield}}{C_i^{raw}} \quad (4)$$

These expressions rely on the char yields of each char samples. In the case of charM, the yield was directly measured during char production. In the case of X0 and Xn (n = 25 or 50) it was obtained from the following equations:

$$\text{X0} \quad \text{Char X0 yield} = \text{CharM yield} \times \text{Char X0 from charM yield} \quad (5)$$

$$\text{Xn (n = 25 or 50)} \quad \text{Char Xn yield} = \text{Char X0 yield} \times \left(1 - \frac{n}{100}\right) \quad (6)$$

where *Char X0 from charM yield* is the char yield between charM and X0 and is measured from TGA results.

The deviation of the mass fraction was calculated as ±20% from the repetition of the analysis on three samples of rice husks and sunflower seed shells. This is due to the combination of the measure uncertainty and of the biomass variability. The uncertainty on the char yield was obtained from the weighing precision and was of approximately 5%. From these values, the relative uncertainty  $u(V_i^{char})$  of the measured volatilization was calculated:

$$\frac{u(V_i^{char})}{V_i^{char}} = \frac{u(C_i^{char})}{C_i^{char}} + \frac{u(char\ yield)}{char\ yield} + \frac{u(C_i^{raw})}{C_i^{raw}} = 45\% \quad (7)$$

### 2.3.5. Scanning electron microscopy coupled to energy dispersive X-ray spectroscopy

Scanning electron microscopy coupled to energy dispersive X-ray spectroscopy (SEM–EDX) was used to study the morphology of the chars and their surface elemental composition. A Philips XL30 microscope was used with a 15 kV electron beam. Secondary electrons (SE) as well as back-scattered electrons (BSE) detection were used. SE detection creates a contrast related to topology while BSE detection creates a contrast related to atomic number. Samples were placed on graphite tape and graphitized before the analysis. For each sample, several particles were observed and EDX was conducted on several points of each particle.

### 2.3.6. Powder X-ray diffraction

Powder X-ray diffraction (P-XRD) was used to identify the crystalline phases in the samples. It was carried out on a Panalytical X'Pert powder diffractometer equipped with a copper anode ( $\lambda K\alpha_1=1.5406 \text{ \AA}$ ,  $\lambda K\alpha_2=1.5444 \text{ \AA}$ ) and an X'Celerator 1D detector. It was configured in Bragg–Brentano geometry, with a variable divergence slit on the primary beam path and a set of anti-scattering slits positioned before and after the sample. Axial divergence was limited by 0.02 rad Soller slits. Samples were placed on zero background holders made from monocrystalline silicon. Phase identification was done using the International Centre for Diffraction Data (ICDD) database on the Panalytical Highscore software.

## 2.4. Thermodynamic equilibrium simulation method

Thermodynamic equilibrium calculations were performed to simulate pyrolysis and gasification in the macroTG. It is well known that biomass gasification at temperatures below 1000 °C is kinetically limited regarding the formation of the gaseous species—CO, CO<sub>2</sub>, CH<sub>4</sub>, H<sub>2</sub> (Kersten et al., 2002). However, for inorganic species in the gas phase, no kinetic limitation has been reported so far except for NH<sub>3</sub> (Kilpinen et al., 1991). The calculations aim to estimate the behavior of the inorganic species, i.e. their volatilization and the fate of the gaseous and condensed phases.

The calculations were performed by minimizing of the Gibbs free energy of the total system with the FactSage 7.2 software and the databases GTOX 5.0, FTsalt and FactPS (Bale et al., 2002; Hack et al., 2012). The initial composition of the system was taken as the mass of each element in the sample and the total mass of the gas used in the experiment. The temperature was the same as the experimental conditions. All initial data are summarized in Table 4. Data for X<sub>n</sub> (n = 25, 50, 75 or 100) initial gas flow are detailed in Table 5: the total gas flow was the sum of the pyrolysis gas (N<sub>2</sub>) and of the gasification gas (mixture of 20vol% H<sub>2</sub>O in N<sub>2</sub>) flows for each species.

Table 4 | Initial data for the thermodynamic equilibrium calculations.

Simulated sample	Temperature	Initial solid	Initial gas
CharM	450 °C	55 g raw rice husks or 40 g raw sunflower seed shells: composition in Table 1	75 g N <sub>2</sub> (1 L.min <sup>-1</sup> , 60 min)
X0	800 °C	150 mg charM: composition in Table 6 and Table 7	25 g N <sub>2</sub> (0.67 L.min <sup>-1</sup> , 30 min)
Xn (n = 25, 50, 75 or 100)	800 °C	150 mg charM: composition in Table 6 and Table 7	See Table 5

Table 5 | Initial gas data for the thermodynamic equilibrium calculations of Xn (n= 25 to 75).

Conversion	Pyrolysis (all biomass species)	Rice husks gasification	Sunflower seed shells gasification
X25	25 g N <sub>2</sub> (0.67 L.min <sup>-1</sup> , 30 min)	10 g N <sub>2</sub> + 1.6 g H <sub>2</sub> O (0.67 L.min <sup>-1</sup> , 15 min)	1 g N <sub>2</sub> + 0.2 g H <sub>2</sub> O (0.67 L.min <sup>-1</sup> , 1.5 min)
X50		28 g N <sub>2</sub> + 4.5 g H <sub>2</sub> O (0.67 L.min <sup>-1</sup> , 42 min)	2 g N <sub>2</sub> + 0.3 g H <sub>2</sub> O (0.67 L.min <sup>-1</sup> , 2.9 min)
X75		62 g N <sub>2</sub> + 10 g H <sub>2</sub> O (0.67 L.min <sup>-1</sup> , 93 min)	3 g N <sub>2</sub> + 0.5 g H <sub>2</sub> O (0.67 L.min <sup>-1</sup> , 4.5 min)
X100		150 g N <sub>2</sub> + 24 g H <sub>2</sub> O (0.67 L.min <sup>-1</sup> , 224 min)	6 g N <sub>2</sub> + 1 g H <sub>2</sub> O (0.67 L.min <sup>-1</sup> , 8.8 min)

The simulation gave results in terms of phases and their composition. The calculated volatilization of each element could be obtained from the elemental composition of the gas phase calculated at equilibrium. The calculated volatilization for charM  $V_{i\text{ calc}}^{\text{charM}}$  was obtained directly (Equation (8)). The calculated volatilization  $V_{i\text{ calc}}^{\text{X0}}$  for X0 and  $V_{i\text{ calc}}^{\text{Xn}}$  for Xn (n = 25, 50, 75 or 100) depended on the measured volatilization for charM  $V_{i\text{ calc}}^{\text{charM}}$  (Equation (9) and Equation (10) respectively). In the case where  $V_{i\text{ calc}}^{\text{charM}}$  was negative, due to uncertainty, its value in the calculation was taken as 0.

$$\text{CharM} \quad V_{i\text{ calc}}^{\text{charM}} = \frac{m_{i\text{ calc}}^{\text{charM gas}}}{m_i^{\text{raw}}} \quad (8)$$

$$\text{X0} \quad V_{i\text{ calc}}^{\text{X0}} = V_{i\text{ calc}}^{\text{charM}} + (1 - V_{i\text{ calc}}^{\text{charM}}) \times \frac{m_{i\text{ calc}}^{\text{X0 gas}}}{m_i^{\text{charM}}} \quad (9)$$

$$\text{Xn (n = 25, 50, 75 or 100)} \quad V_{i\text{ calc}}^{\text{Xn}} = V_{i\text{ calc}}^{\text{charM}} + (1 - V_{i\text{ calc}}^{\text{charM}}) \times \frac{m_{i\text{ calc}}^{\text{Xn gas}}}{m_i^{\text{charM}}} \quad (10)$$

with:

$m_{i\text{ calc}}^{\text{charM gas}}$  the calculated mass of element i in the gas phase for charM;

$m_{i\text{ calc}}^{\text{X0 gas}}$  the calculated mass of element i in the gas phase for X0;

$m_{i\text{ calc}}^{\text{Xn gas}}$  the calculated mass of element i in the gas phase for Xn (n = 25, 50, 75 or 100);

$m_i^{\text{raw}}$  the measured mass of element i in the raw biomass;

$m_i^{charM}$  the measured mass of element i in charM;

$V_i^{charM}$  the measured volatilization of element i during charM production (0 if negative).

### 3. Results and discussion

#### 3.1. Gasification kinetic profiles

Gasification solid conversions of the chars produced from rice husks and sunflower seed shells in the macroTG are plotted versus time in Figure 4. The profiles obtained through TGA are also plotted for comparison. Results are also plotted as the solid conversion rate versus the conversion in Figure 5.

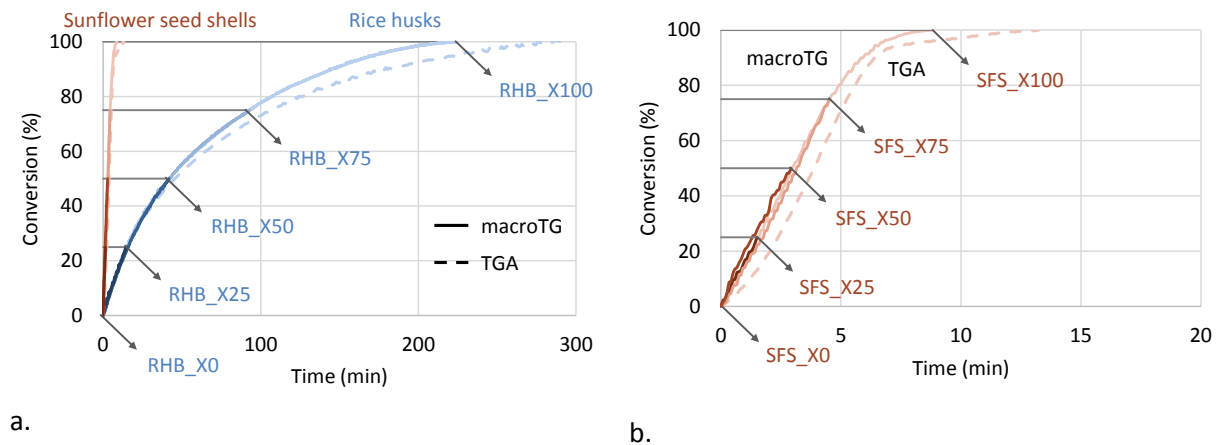


Figure 4 | a. Gasification solid conversion of the rice husk and sunflower seed shell chars as a function of time. b. Zoom on sunflower seed shells.

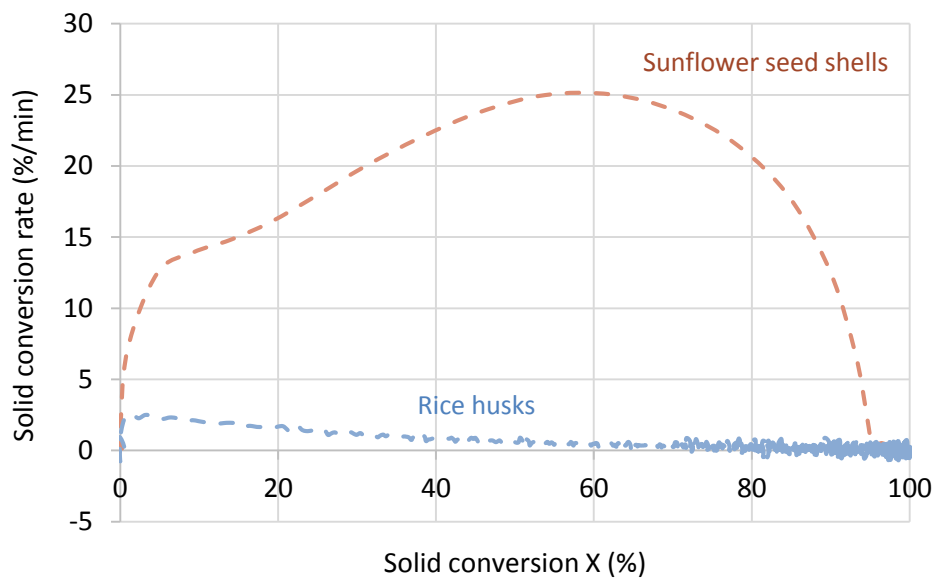


Figure 5 | Solid conversion rate as a function of the conversion for rice husks and sunflower seed shells in the TGA.

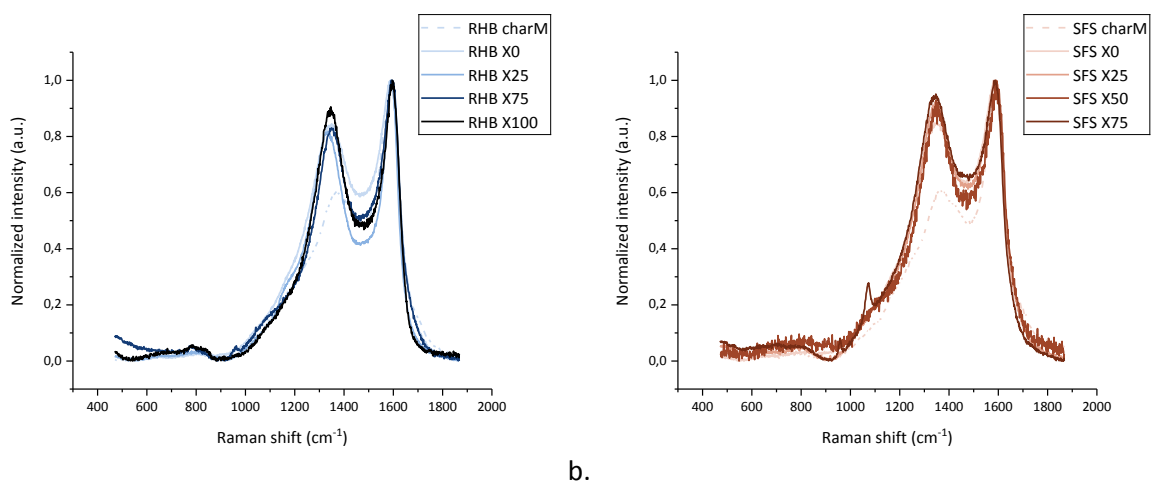
For both biomass samples, their kinetic behavior in macroTG was similar to their behavior in TGA. Rice husks gasified slowly— $1.4 \text{ \%} \cdot \text{min}^{-1}$  average reactivity (Table 1)—and had a decreasing gasification rate along conversion (Figure 5). Sunflower seed shells gasified fast— $30.3 \text{ \%} \cdot \text{min}^{-1}$  average reactivity (Table 1)—and had a gasification rate that decreased at high conversion values (Figure 5).

Moreover, good repeatability was observed for each biomass in the macroTG. However, fast cooling could not be carried out which resulted in an additional mass loss under inert atmosphere. This additional mass loss was measured as 10-15% of the initial ash-free mass of rice husks and 20-25% of sunflower seed shells. This observation must be kept in mind when discussing the results of the sample characterizations.

### 3.2. Results of the characterization of the char carbon matrix

#### 3.2.1. Structure of the carbon matrix

The structure of the char carbon matrix was investigated through Raman spectroscopy. Typical Raman spectra obtained for rice husk and sunflower seed shell chars are presented in Figure 6. To allow comparison, intensities were normalized by setting the maximum intensity—at the Raman shift of the center of the G band—to 1.



a. b.  
Figure 6 | Normalized Raman spectra of a. rice husk chars and b. sunflower seed shell chars at several pyrolysis and gasification conversions.

Carbon could still be detected in sample RHB\_X100 which indicates that gasification was not completely carried out until completion.

The Raman spectra analysis was supplemented by the calculation of peak intensity ratios. The evolution of the peak intensity ratios during conversion is shown in Figure 7.

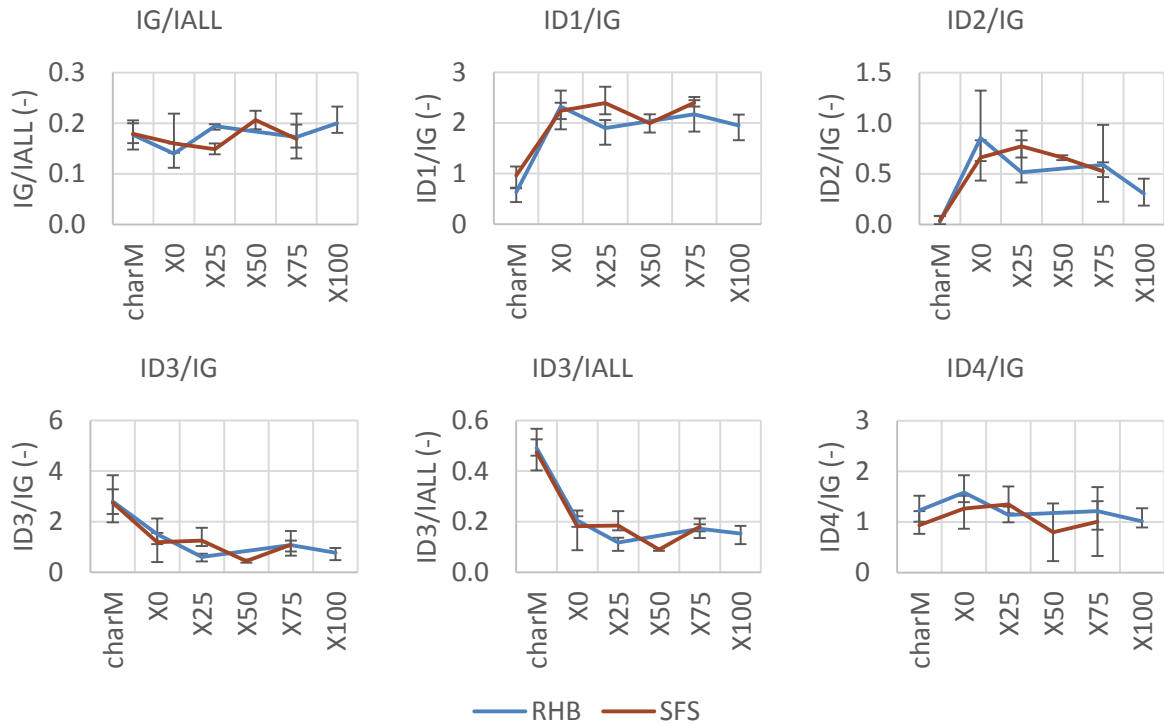


Figure 7 | Evolution of the peak intensity ratios during pyrolysis and gasification conversion of rice husk and sunflower seed shell chars.

For both biomass samples, the only noticeable changes occurred when the pyrolysis temperature increased from 450 °C (charM) to 800 °C (X0). When the pyrolysis temperature increased there was an increase of the D1 and D2 band intensities and a decrease of the D3 band intensity. This suggests that the amorphous carbon structures became more organized and formed graphene layers. The latter seemed to be independent and not to stack on top of each other. This is in accordance with literature observations for biomass and coal chars (Guizani et al., 2017; Wang et al., 2016; Zhao et al., 2016).

No significant difference could be observed between the spectra acquired at various gasification conversion rates. Variations were in the range of the measurement uncertainty and were significantly inferior to the variations between the two pyrolysis temperatures.

More importantly, when comparing the two biomass samples at each conversion value, no significant difference could be observed either. This result shows that the structural properties of the carbon matrix of the chars do not explain the difference in gasification reactivity that exists between the two types of biomass.

### 3.2.2. Porosity of the carbon matrix

The porosity of the carbon matrix was first investigated through N<sub>2</sub> adsorption. N<sub>2</sub> adsorption isotherms of rice husk and sunflower seed shell chars during pyrolysis and gasification conversion are presented in Figure 8.

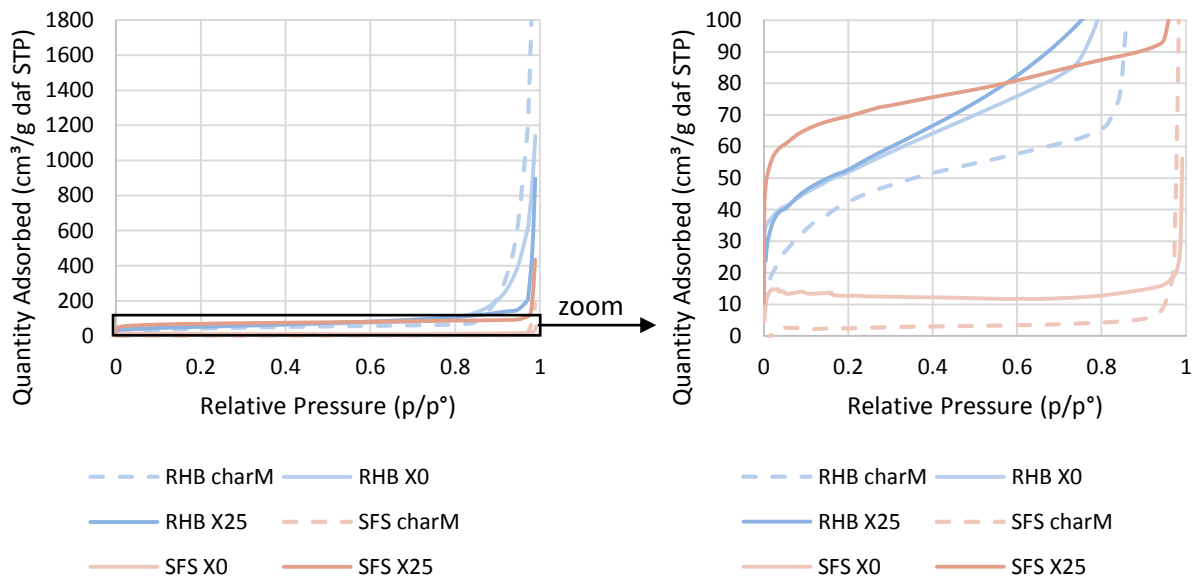


Figure 8 | N<sub>2</sub> adsorption isotherms of rice husk and sunflower seed shell chars at several pyrolysis and gasification conversions.

N<sub>2</sub> adsorption isotherms could not be obtained for chars from gasification at 50% conversion and above for either biomass indicating no or small porosity. Isotherms obtained from N<sub>2</sub> adsorption on chars from pyrolysis and gasification at 25% conversion were IUPAC type I (Thommes et al., 2015) indicating that the char samples were mainly microporous for both biomass types.

N<sub>2</sub> adsorption can only measure large micropores (1-2 nm), mesopores (2-50 nm) and macropores (>50 nm). Therefore a narrower porosity, i.e. ultramicroporosity (<1 nm), was evaluated through CO<sub>2</sub> adsorption, as the CO<sub>2</sub> molecule (0.33 nm) is smaller than the N<sub>2</sub> molecule (0.36 nm) (Tascón, 2012). Results for both biomass types are presented in Figure 9.

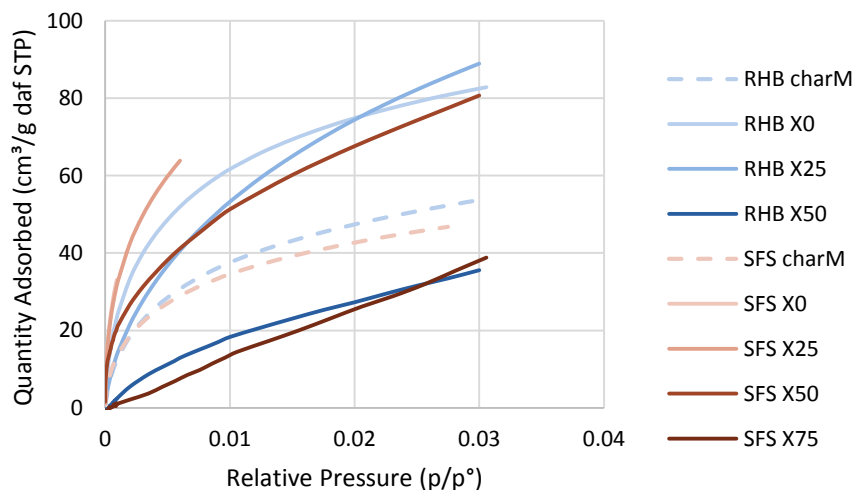


Figure 9 | CO<sub>2</sub> adsorption isotherms of rice husk and sunflower seed shell chars at several pyrolysis and gasification conversions.

Resulting N<sub>2</sub> and CO<sub>2</sub> adsorption isotherms were analyzed using the DFT model to obtain a pore size distribution for each sample. It is presented in Figure 10 expressed in terms of incremental area, with a focus on narrow pores measured from CO<sub>2</sub> adsorption in Figure 11.

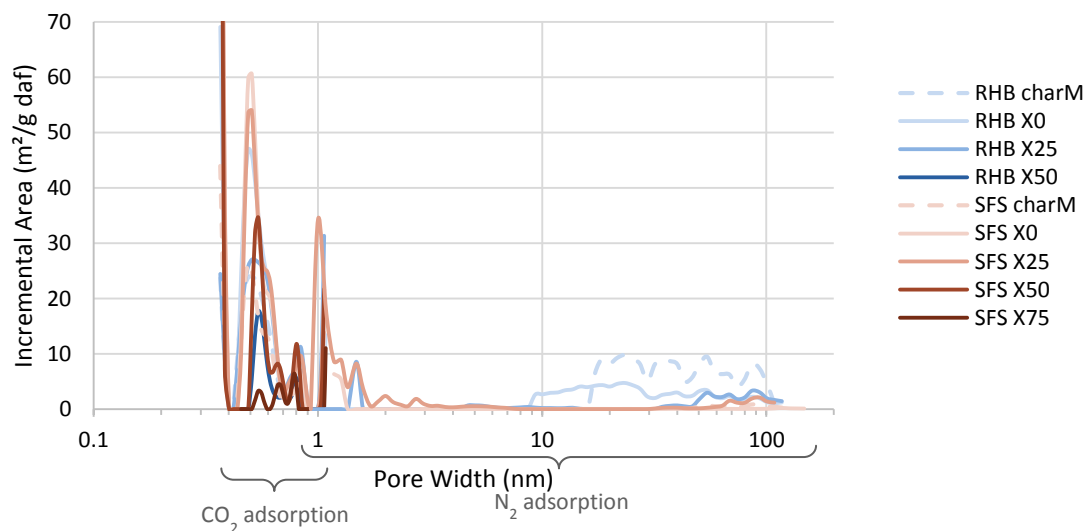


Figure 10 | Pore size distribution using DFT model from N<sub>2</sub> and CO<sub>2</sub> adsorption isotherms of rice husk and sunflower seed shell chars at several pyrolysis and gasification conversions expressed in terms of incremental area.

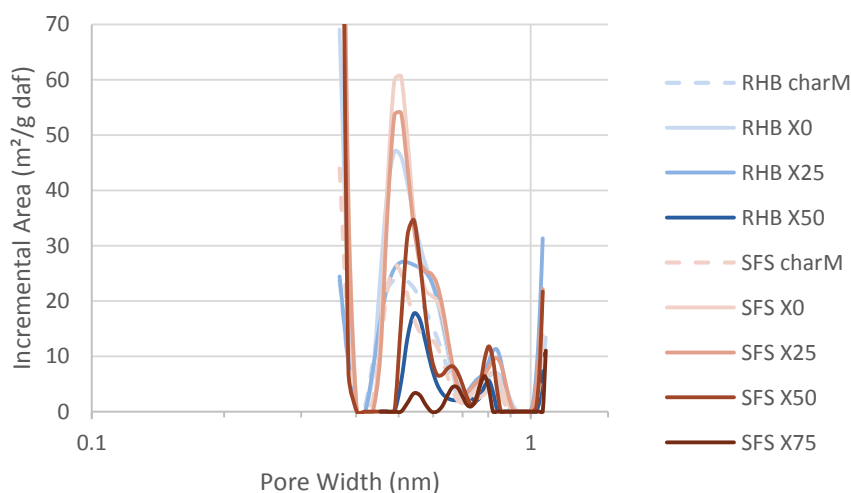


Figure 11 | Ultramicropore size distribution using DFT model from CO<sub>2</sub> adsorption isotherms of rice husk and sunflower seed shell chars at several pyrolysis and gasification conversions expressed in terms of incremental area.

For both biomass types, when the pyrolysis temperature increased from 450 °C (charM) to 800 °C (X0), the ultramicroporosity (< 1 nm) area increased and there was no or low wider porosity. This corresponds to the opening of new ultramicropores during the devolatilization. During gasification, the ultramicroporosity area decreased in favor of wider microporosity (around 1 nm), while mesoporosity and macroporosity remained low. This behavior suggests a coalescence of the ultramicropores into wider micropores during the char interaction with the gasifying agent. To our knowledge, there is no study available on the evolution during gasification of the ultramicroporosity measured by CO<sub>2</sub> adsorption in the gasification literature. However, this technique is in use in the field of activated carbons. The physical activation process is equivalent to a gasification. The results obtained in the present study are in accordance with the observations reported in the activated carbon literature (Rodríguez-Reinoso et al., 1995).

When comparing biomass types, for the chars from pyrolysis charM and X0, sunflower seed shells and rice husks had similar micro- and ultramicroporosity areas. Rice husks had a higher macroporosity area, though it remained low (Figure 10). For the chars from gasification, the ultramicroporosity area of rice husks (slow gasifying biomass) was lower than sunflower seed shells (fast gasifying biomass)—almost half. Their wider porosity was similar. This difference in terms of ultramicroporosity could be linked to the difference in terms of gasification reactivity. Indeed, a lower ultramicroporosity area in the case of rice husks could be related to their slower gasification due to a reduced reacting surface. However, the ultramicroporosity of both biomass chars at steam injection—i.e. X0 samples—were similar and the differences only occurred during gasification (Figure 11). This indicates that the porosity properties are not the cause of the differences between the gasification reactivities of the biomass samples, but rather a consequence of another mechanism.

### 3.2.3. Surface chemistry of the carbon matrix

The surface chemistry of the carbon matrix was characterized through TPD–MS. Cumulative gas desorption between 24 and 800 °C during TPD–MS of rice husk and sunflower seed shell chars at several pyrolysis and gasification conversions is presented in Figure 12. Samples SFS\_X50 and SFS\_X75 could not be analyzed due to low char amounts.

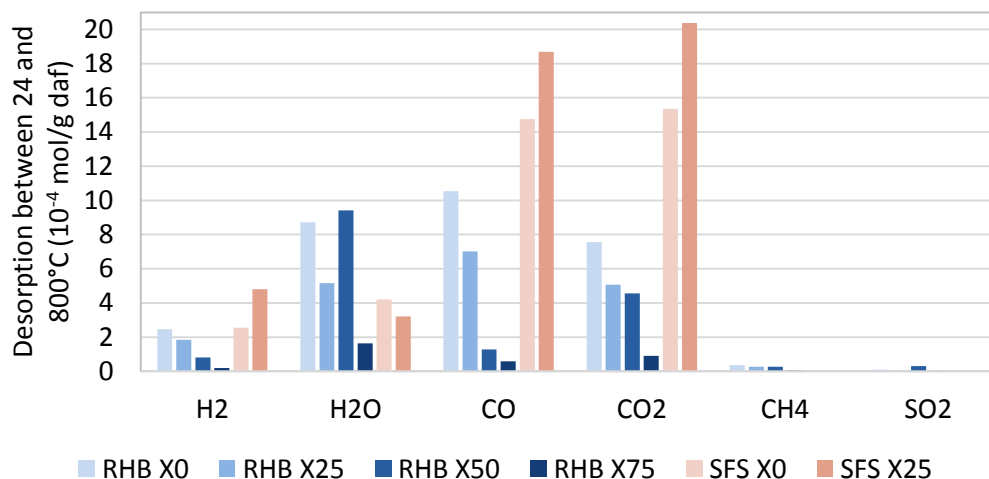


Figure 12 | Cumulative gas desorption between 24 and 800 °C during TPD–MS of rice husk and sunflower seed shell chars at several gasification conversions.

Sunflower seed shell chars released much more CO and CO<sub>2</sub> than rice husk chars. Another noticeable difference between the two biomass types was the gas desorption evolution during gasification conversion. For rice husk chars gas desorption decreased during conversion, except H<sub>2</sub>O, while for sunflower seed shell chars it seemed to increase, except for H<sub>2</sub>O. In addition, a slight desorption of CH<sub>4</sub> and SO<sub>2</sub> was observed for rice husks, but not for sunflower seed shells. Both biomass species had the same S content (Table 1). Therefore, this TPD-MS result indicate that this element occurred in a different form in both biomass species and behaved differently.

The detail of the desorption of each released gas as a function of temperature is presented in Figure 13 at several pyrolysis and gasification conversions for the two biomass types. It is to be noted that the scale of desorption rate is different for each desorbed gas.

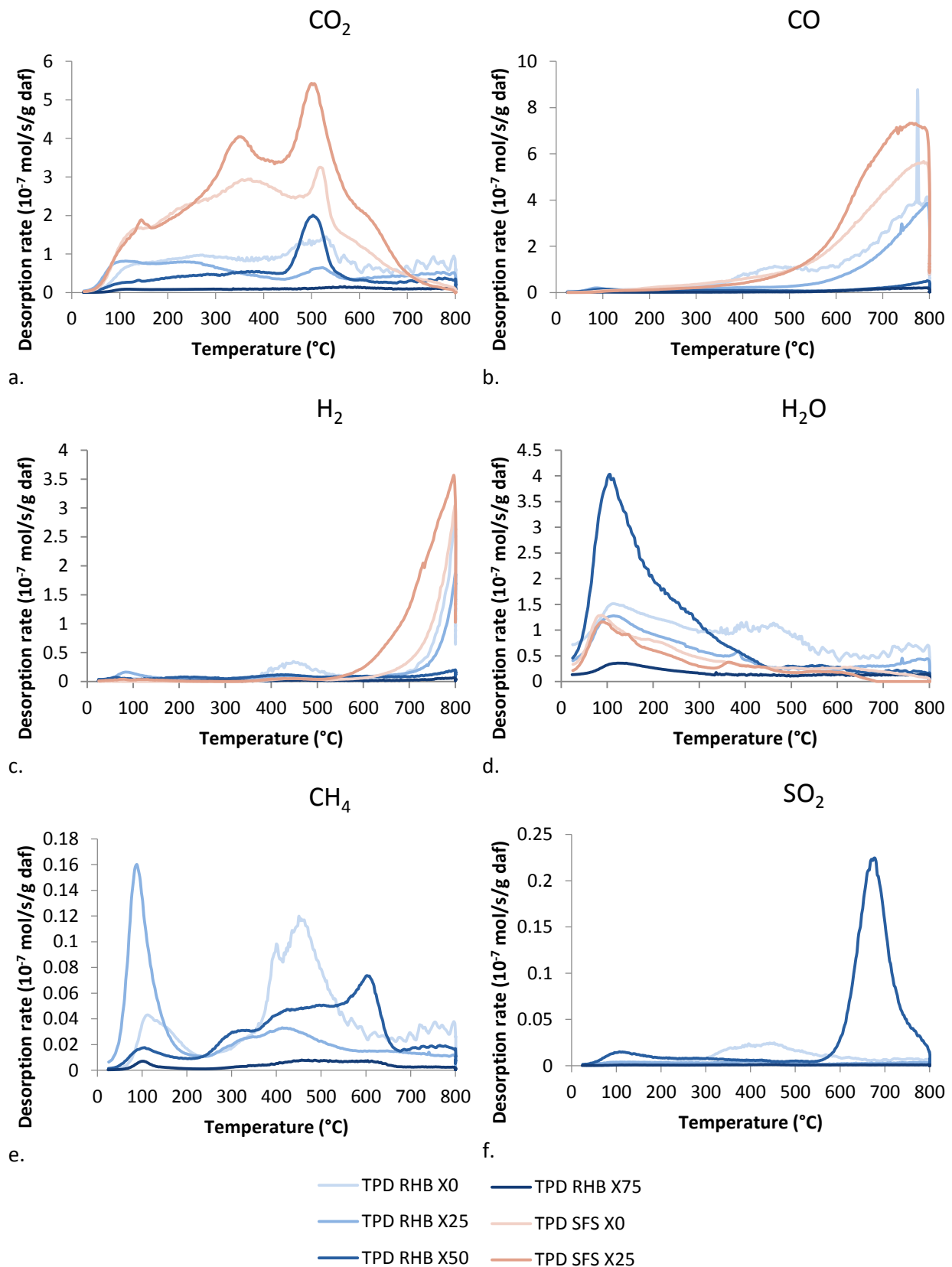


Figure 13 | a.  $\text{CO}_2$ , b.  $\text{CO}$ , c.  $\text{H}_2$ , d.  $\text{H}_2\text{O}$ , e.  $\text{CH}_4$  and f.  $\text{SO}_2$  desorption during TPD-MS of rice husk and sunflower seed shell chars at several pyrolysis and gasification conversions.

Desorption was of the same order of magnitude and occurred around the same temperatures as what has been observed in literature for gasification chars (Guizani et al., 2016).

The gases desorption is due to the decomposition of the carbon surface groups that occur on specific temperature ranges. Desorption occurred at the same temperatures for both biomass types. Therefore, the functional groups in chars from both biomass types were similar. Functional groups also remained similar along gasification conversion.

At low temperature—i.e. below 400 °C, CO<sub>2</sub> and H<sub>2</sub>O were released (Figure 13a. and d.). It corresponds to the decomposition of carboxyles. They either directly decomposed to CO<sub>2</sub> or dehydrated to form lactones and anhydrides (Figueiredo et al., 1999; Guizani et al., 2016). These groups then decomposed to CO<sub>2</sub>, as well as CO for anhydrides, until around 600 °C (Figure 13a. and b.). Then, CO was produced at higher temperatures (Figure 13b.). It resulted from the decomposition of ethers, phenol, carbonyls and quinones (Figueiredo et al., 1999; Guizani et al., 2016). H<sub>2</sub> was also observed at high temperatures—i.e. above 700 °C (Figure 13c.). It originated in the thermal decomposition of C – H bonds (Guizani et al., 2016).

In conclusion, the only difference between the two biomass types was the concentration—and not the nature—of surface functions, with a higher concentration in the case of sunflower seed shell chars. This evolution of this property follows the evolution of the microporosity: sunflower seed shells also have a higher microporosity. The similar evolution of the microporosity and of the surface functions concentration has also been observed in literature (Arriagada et al., 1997).

### 3.3. Results of the characterization of the inorganic fraction of the chars

#### 3.3.1. Volatilization of the main inorganic elements

The inorganic elemental composition of the charM, X0, X25 and X50 samples was analyzed by ICP–AES. Results are presented in Table 6 and Table 7 for rice husks and sunflower seed shells respectively, and compared to raw biomass values. From these measurements, the measured volatilization of the three main inorganic elements of each biomass species during pyrolysis was obtained (Equation (4)). Values are given in Table 8.

Table 6 | Inorganic element content and char yield of raw, charM, X0, X25 and X50 rice husk samples (in dry basis).

Sample	Raw RHB	RHB charM	RHB X0	RHB X25	RHB X50	
Char yield (%)	100	42	38**	28***	14***	
C	} (wt%)	41.6	57.1	—	—	—
H		5.2	3.3	—	—	—
O*		45.1	23	—	—	—
N		0.5	0.8	—	—	—
S	} (mg.kg <sup>-1</sup> )	1000	1840	—	—	—
Cl		1016	325	—	—	—
Si		63955	130000	141000	199000	411000
K		5822	15000	17000	23000	48000
Ca		1797	4000	4000	7000	12000
Mg		659	1000	2000	2000	4000
P		981	2000	2000	2000	5000
Na		413	<1000	<1000	—	—
Al		228	<1000	<1000	—	—
Fe		192	1000	<1000	—	—
Main inorganic elements	Si – K – Ca	—	—	—	—	

\*Total (i.e. organic and inorganic) oxygen calculated by difference with all other elements.

\*\*Calculated from Equation (5) with *Char X0 from charM yield = 90%* measured from TGA results.

\*\*\*Calculated from Equation (6).

Table 7 | Inorganic element content and char yield of raw, charM, X0, X25 and X50 sunflower seed shell samples (in dry basis).

Sample	Raw SFS	SFS charM	SFS X0	SFS X25	SFS X50	
Char yield (%)	100	32	28**	21***	11***	
C	} (wt%)	50.2	76.6	—	—	—
H		6.5	3.8	—	—	—
O*		40.6	12.4	—	—	—
N		0.7	1.2	—	—	—
S	} (mg.kg <sup>-1</sup> )	1000	1180	—	—	—
Cl		1000	959	—	—	—
Si		194	<1000	19000	<1000	10000
K		9729	27000	29000	15000	20000
Ca		4489	13000	14000	15000	<1000
Mg		1838	6000	6000	6000	28000
P		896	3000	2000	2000	6000
Na		9	<1000	2000	—	—
Al		150	<1000	2000	—	—
Fe		1099	5000	5000	—	—
Main inorganic elements	K – Ca – Mg	—	—	—	—	

\*Total (i.e. organic and inorganic) oxygen calculated by difference with all other elements.

\*\*Calculated from Equation (5) with *Char X0 from charM yield = 88%* measured from TGA results.

\*\*\*Calculated from Equation (6).

Table 8 | Volatilization of the main inorganic elements measured for raw biomass, charM, X0, X25 and X50 for both species.

Volatilization	RHB				SFS			
	charM	X0	X25	X50	charM	X0	X25	X50
Si	15%	17%	12%	9%	—	—	—	—
K	-8%	-10%	-11%	-16%	11%	16%	68%	78%
Ca	7%	16%	-10%	6%	7%	12%	30%	98%
Mg	—	—	—	—	-4%	8%	31%	-60%

The volatilization of the main inorganic elements Si, K, Ca and Mg are shown in Figure 14 for rice husks and sunflower seed shells.

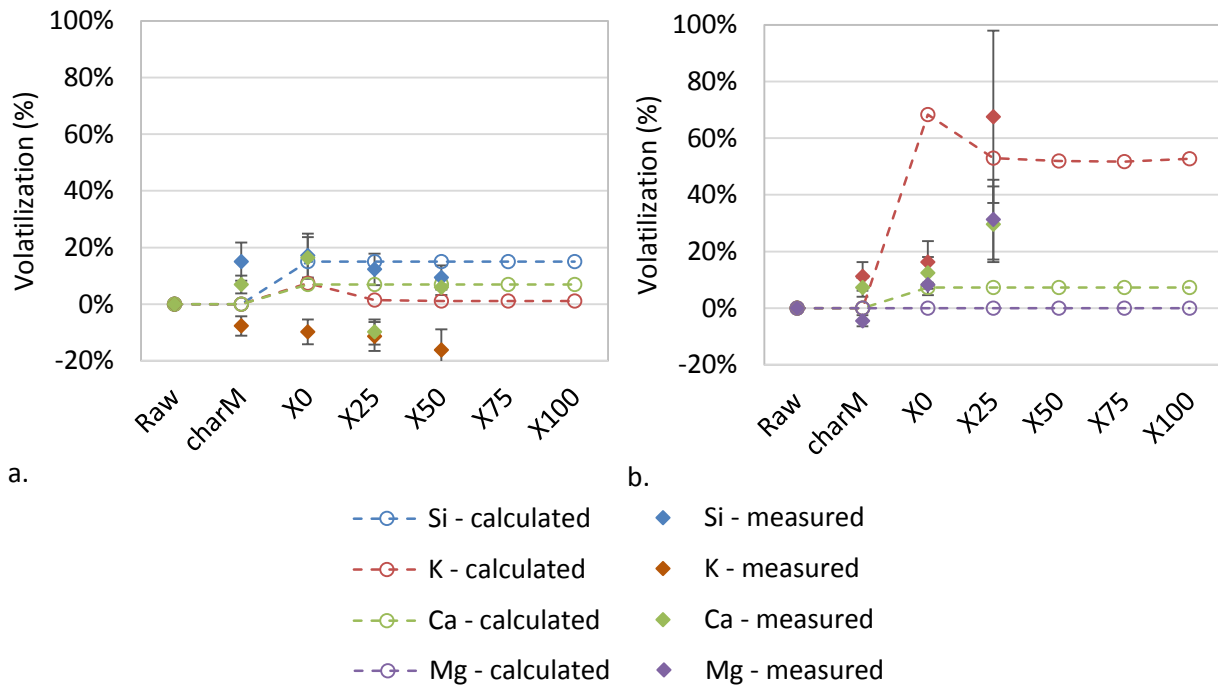


Figure 14 | Calculated and measured volatilization of the three main inorganic elements a. Si, K and Ca in the rice husk samples, and b. K, Ca and Mg in the sunflower seed shell samples.

For both biomass species, calculations predicted that no volatilization would occur in the case of charM at 450 °C. Then for X0 samples pyrolyzed at 800 °C and for all gasified samples, the volatilization remained non-existent or low (< 20%) except for K in sunflower seed shells. In this last case, the calculated volatilization was above 50%. From the calculated volatilization of Cl, it probably formed KCl. However, it could not form only KCl since in sunflower seed shells the molar ratio K/Cl was of 8.8 (calculated from data in Table 7) and was superior to the molar ratio of 1 from KCl. Calculations showed that K was released in the form of KOH(g), K(g) and KCl(g).

From the measures on rice husks samples, no significant volatilization of the main inorganic elements was detected during both the pyrolysis and the gasification steps. This is in accordance with the calculation at thermodynamic equilibrium. Authors in literature also observed the lack of or low volatilization during pyrolysis (Dirbeba et al., 2016; Lane et al., 2015).

In the case of sunflower seed shells, no significant volatilization of the main inorganic elements was detected during the pyrolysis step—i.e. for SFS\_charM and SFS\_X0. This is in accordance with calculated volatilizations during pyrolysis. Then, during gasification, K was volatilized as predicted by calculations at thermodynamic equilibrium while Ca and Mg remained in the condensed phases.

In conclusion, when looking at the main inorganic elements Si, K, Ca and Mg alone and not the compounds they form, the chars at the end of pyrolysis were not different from the initial raw biomass. Then, during gasification, only K from sunflower seed shells was volatilized. Mg as well as the main elements of rice husks Si, K and Ca remain in condensed phases.

### 3.3.2. Determination of the inorganic condensed phases

The elements forming the inorganic fraction are an important data. However, it is essential to also characterize the condensed phases they form in order to understand the role of the inorganic

fraction in the gasification mechanisms. Indeed, the same element can be active or not depending on the condensed phase it forms. For example, potassium has a catalytic activity on gasification in KOH or  $K_2CO_3$ , but not when it forms K-silicates (Arnold and Hill, 2019).

SEM–EDX analysis showed that for each biomass type the chars consisted of various phases. It is a semi-quantitative method that only allows local observations. It can be noted that, with a BSE detection, phases containing mainly carbon (i.e. the carbon matrix) appeared clearly as dark phases while inorganic phases appeared lighter due to the atomic number contrast.

In the case of rice husks, char samples comprised a carbonaceous matrix without any inorganic element whose quantity seemed to decrease during conversion as expected. The second main phase in rice husk chars was  $SiO_2$  that appeared in the form of grains, often with a characteristic bumpy shape as described in literature for ash and raw biomass (Ganesh et al., 1992; Krishnarao et al., 2001; Park et al., 2003; Ryu et al., 1997). Other phases that did not appear as proper grains could be observed. They were constituted of K, Si and O, and were, therefore, probably K-silicates. These phases sometimes also contained Ca. However, Ca was observed in few samples even though it was the third main element contained in rice husks after Si and K. This can be explained by the fact that SEM–EDX is a technique that analyses the chars locally. Therefore, dispersed compounds, which can be the case of Ca-compounds, can be difficult to locate. In addition, silicates were found in smooth phases which indicates that it was liquid at the process temperature. An example of SEM images is given in Figure 15 for RHB\_X0 with SE (topology contrast) and BSE (atomic number contrast) detection.

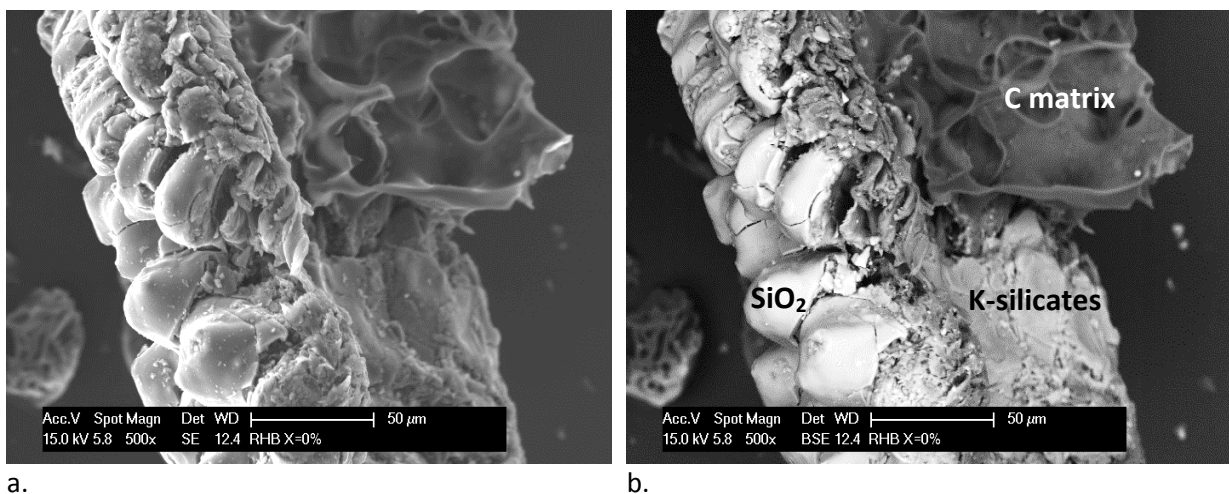


Figure 15 | SEM image of a char particle from RHB\_X0 with a. SE detection and b. BSE detection.

In the case of sunflower seed shell chars, the carbonaceous matrix often contained some K and sometimes also some Ca. Smooth phases were observed that contain K, Ca and/or Mg with O and maybe C which could not be seen because of the sample graphitization. They were probably carbonate phases. Phases containing K, S and O could also be found. KCl was also present at the surface of the chars in the form of flakes or grains distinct from the matrix. In addition, grains containing Fe, Cr and Ni could be observed which most likely indicates a pollution by stainless steel. It might have originated from shell grinding or pelletization. An example of SEM image is given in Figure 16 for SFS\_X25 with SE and BSE detection.

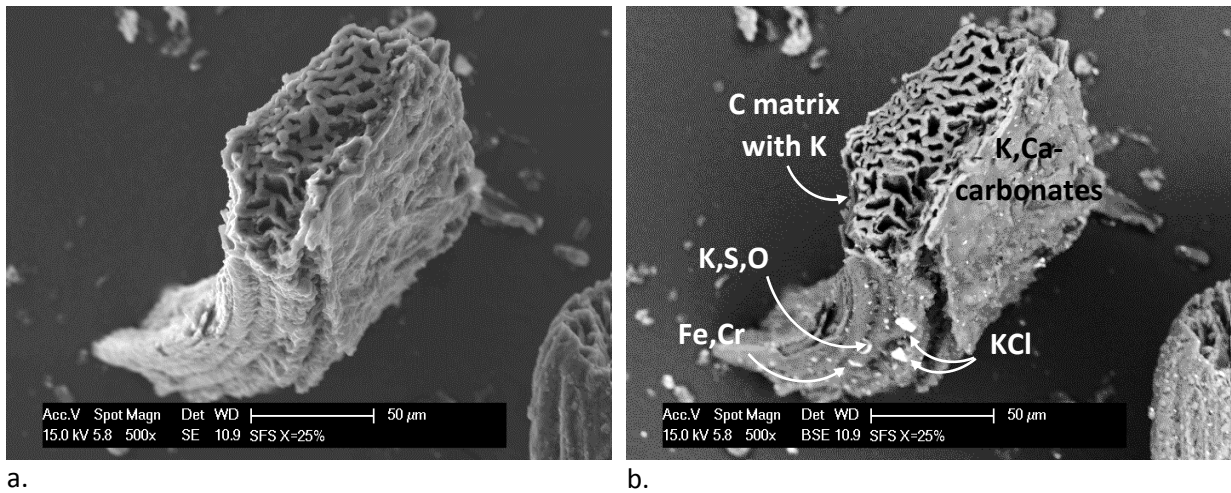


Figure 16 | SEM image of a char particle from SFS\_X25 with a. SE detection and b. BSE detection.

SEM–EDX analysis was completed with P-XRD analysis to investigate the crystalline inorganic compounds.

The evolution of the P-XRD diffractograms at several pyrolysis and gasification conversions is presented in Figure 17 for rice husks and in Figure 18 for sunflower seed shells. The identified phases are summarized in Table 9 and Table 10.

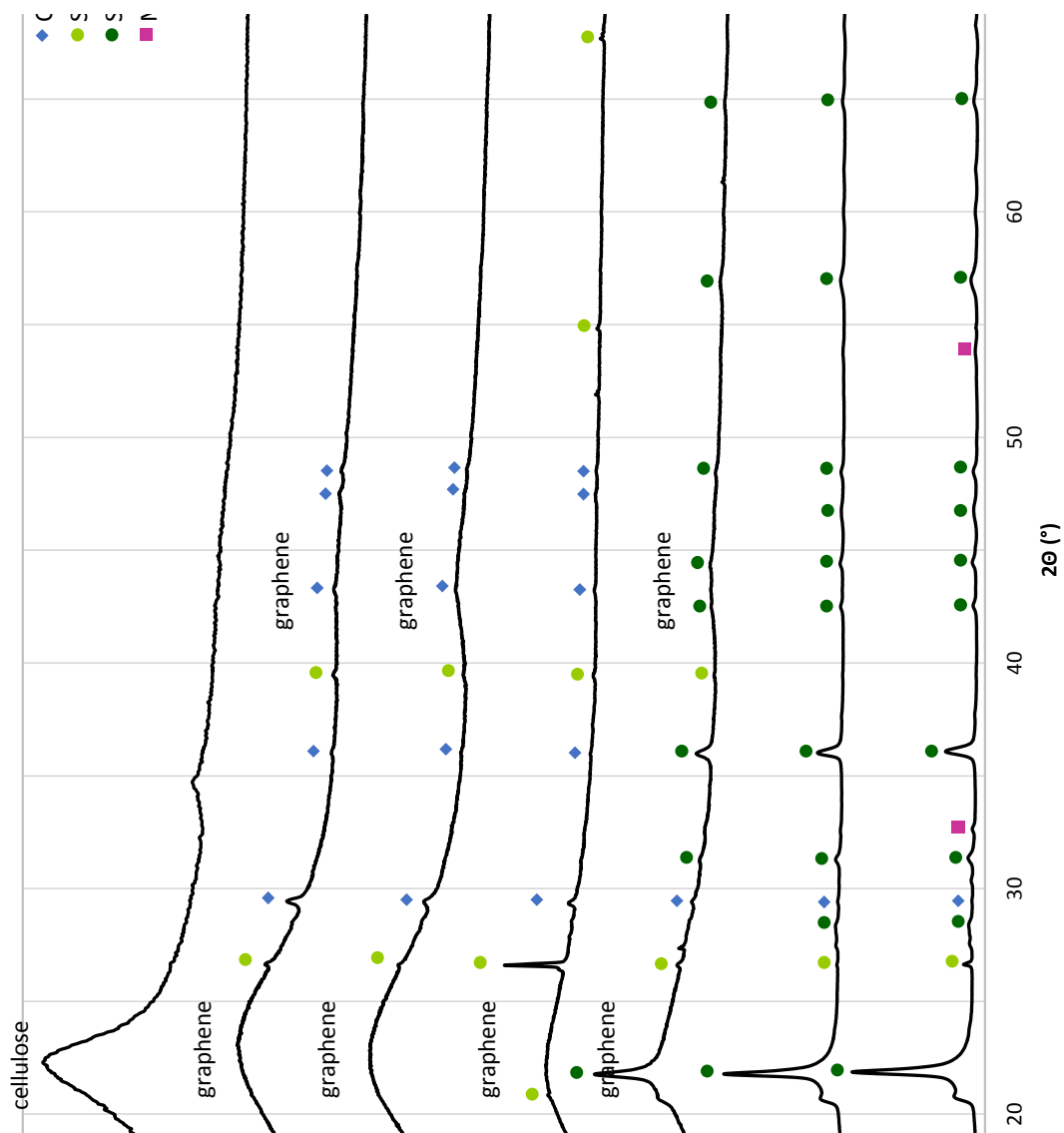


Figure 17 | P-XRD diffractograms of rice husk chars at several pyrolysis and gasification conversions.

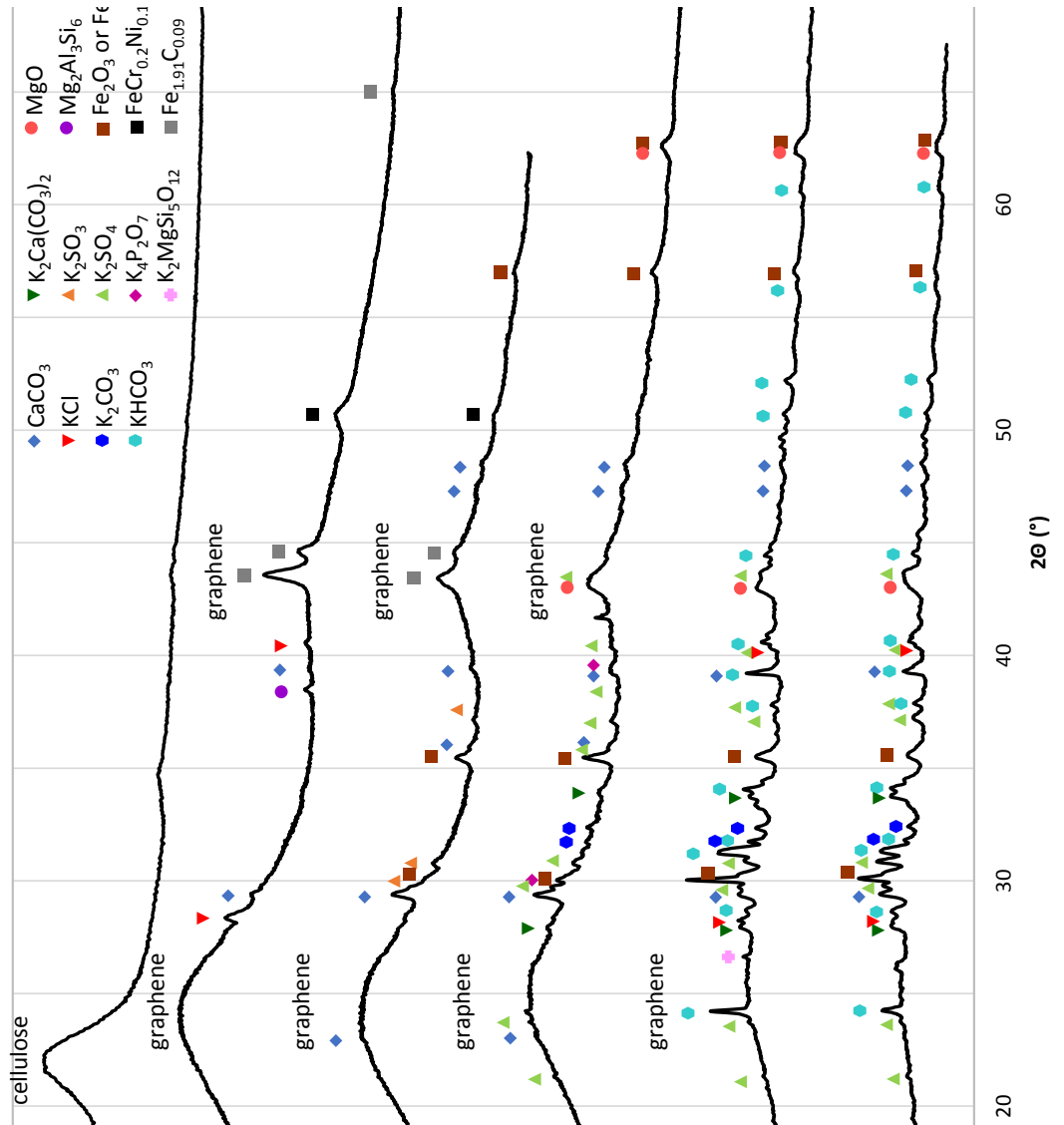


Figure 18 | P-XRD diffractograms of sunflower seed shell chars at several pyrolysis and gasification conversions.

Table 9 | List of inorganic compounds identified in rice husks biomass and chars.

	Rice husks Si – K – Ca						
	Raw	CharM	X0	X25	X50	X75	X100
Cellulose	x						
Graphene		x	x	x	x		
Liquid			o	o	o	o	o
SiO <sub>2</sub> quartz	o	x	x	x	x	x	x
SiO <sub>2</sub> opal or cristobalite+tridymite					x	x	x
K silicates	o	o	o	o	o	o	o
Ca-K silicates		o		o			o
Ca silicates	o						
CaCO <sub>3</sub>		x	x	x	x	x	x
MgCO <sub>3</sub>							x

x Characterized by P-XRD.

o Local elemental observations only, i.e. characterized through SEM–EDX.

Table 10 | List of inorganic compounds identified in sunflower seed shell biomass and chars.

	Sunflower seed shells K – Ca – Mg						
	Raw	CharM	X0	X25	X50	X75	X100*
Cellulose	x						
Graphene		x	x	x	x	x	
CaCO <sub>3</sub>	o	x	x	x	x	x	
K <sub>2</sub> Ca(CO <sub>3</sub> ) <sub>2</sub>	o	o	o	x	x	x	
Ca-K-Mg carbonates		o	o		o	o	o
K <sub>2</sub> CO <sub>3</sub>				x	x	x	
KHCO <sub>3</sub>					x	x	
KCl		x			x	x	
K <sub>2</sub> SO <sub>3</sub>	o		x				
K <sub>2</sub> SO <sub>4</sub>				x	x	x	
K <sub>4</sub> P <sub>2</sub> O <sub>7</sub>				x			
K <sub>2</sub> MgSi <sub>5</sub> O <sub>12</sub>					x		
MgO				x	x	x	
Mg <sub>2</sub> Al <sub>3</sub> Si <sub>6</sub>		x					
Fe <sub>1.91</sub> C <sub>0.09</sub>	o	x	x				
FeCr <sub>0.2</sub> Ni <sub>0.16</sub> C <sub>0.06</sub>	o	x	x				
Fe <sub>3</sub> O <sub>4</sub>			x	x	x	x	o

x Characterized by P-XRD.

o Local elemental observations only, i.e. characterized through SEM–EDX.

The broad peaks observed for both raw biomass samples correspond to partially ordered cellulose and are typical of raw biomass P-XRD diffractograms (Vassilev et al., 2012). The two broad peaks around  $2\theta = 23^\circ$  and  $44^\circ$  in char diffractograms correspond to graphene layers (Saavedra Rios et al., 2018).

P-XRD analysis of rice husk chars confirmed the presence of Si in the SiO<sub>2</sub> form. SiO<sub>2</sub> was found as quartz in all samples. From 50% conversion another form of SiO<sub>2</sub> appeared. However, the data did not allow to conclude on the exact form. The new SiO<sub>2</sub> phase could have been opal, which is poorly referenced in the diffractograms database and is not a pure structure but a combination of

cristobalite, tridymite and hydrated amorphous silica. It could also have been cristobalite, which was properly identified, and tridymite, for which a peak at  $2\theta = 23^\circ$  did not appear here.  $\text{CaCO}_3$  as well as  $\text{MgCO}_3$  for RHB\_X100 were also present in the chars but were not observed with SEM–EDX. This can be explained by the fact that SEM–EDX is a technique that analyses the chars locally and  $\text{CaCO}_3$  was a minor compound. No K-compound was identified through this technique, while K was the second main inorganic element contained in rice husks. This can be explained by the fact that P-XRD only detects crystalline phases so K-compounds might have been present in non-crystalline forms.

P-XRD analysis of sunflower seed shell chars also confirmed some phases observed during SEM–EDX analysis: KCl; carbonates identified as  $\text{CaCO}_3$ ,  $\text{K}_2\text{CO}_3$ ,  $\text{KHCO}_3$  and  $\text{K}_2\text{Ca}(\text{CO}_3)_2$ ; K-, S- and O-containing phases identified as  $\text{K}_2\text{SO}_3$  and  $\text{K}_2\text{SO}_4$ ; Mg-containing phases mainly identified as MgO; steel in the form of  $\text{FeCr}_{0.2}\text{Ni}_{0.16}\text{C}$  and  $\text{Fe}_{1.91}\text{C}_{0.09}$  that seemed to be oxidized to  $\text{Fe}_2\text{O}_3$  or  $\text{Fe}_3\text{O}_4$  at the end of the gasification reaction.

Raman spectra at high conversion also confirmed some of the compounds identified through SEM–EDX and P-XRD analyses. In some repetitions of the spectra, peaks appeared that were not related to carbon structure and therefore correspond to inorganic compounds. A spectrum with such peaks is shown in Figure 19a. for rice husk char sample RHB\_X100 and in Figure 19b. for sunflower seed shell char sample SFS\_X75.

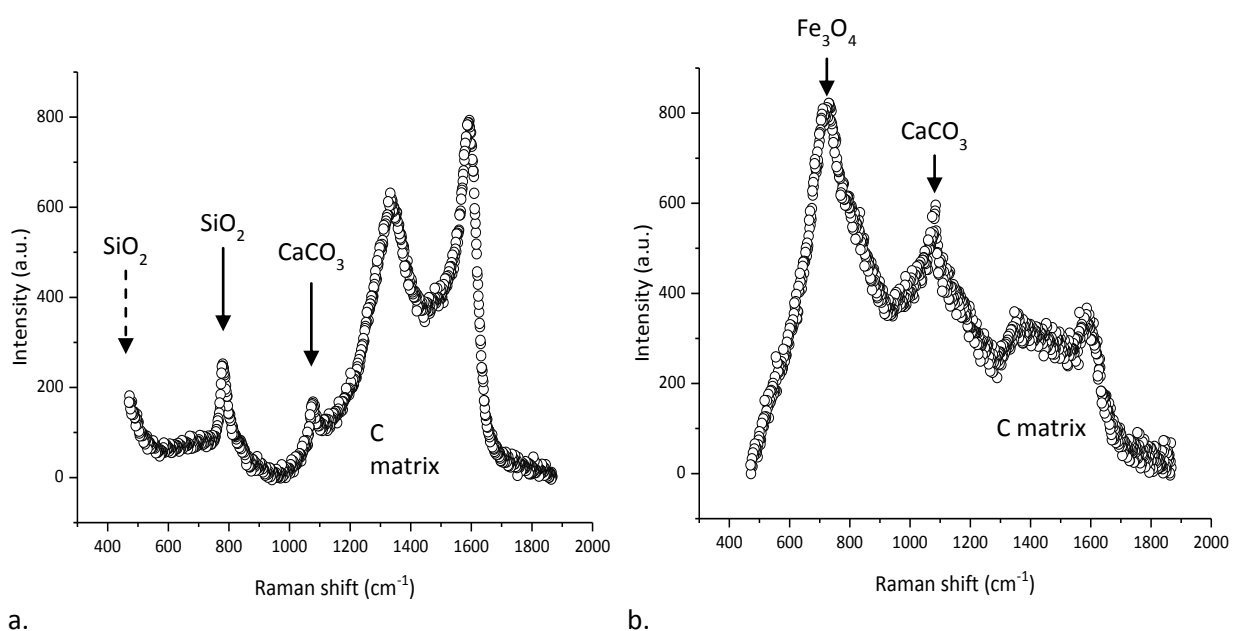


Figure 19 | Raman spectra showing inorganic compounds of the sample a. RHB\_X100 and b. SFS\_X75.

For both biomass species,  $\text{CaCO}_3$  was clearly identified. Raman data also permitted to identify the iron oxide present in sunflower seed shell char samples as  $\text{Fe}_3\text{O}_4$  and not  $\text{Fe}_2\text{O}_3$ . Lastly, the peak at  $800 \text{ cm}^{-1}$  in spectra from rice husk chars can correspond to a weak peak of  $\text{SiO}_2$  cristobalite or tridymite that have similar patterns, but their main peak is around  $420\text{--}430 \text{ cm}^{-1}$ , which is out of the recorded Raman shift range.

### 3.4. Results summary

When characterizing the char carbon matrix, both biomass species had similar porosity before steam injection and carbon structures. Therefore, these properties do not justify the reactivity difference between them. Nevertheless, there was a higher microporosity and quantity of surface functions during steam gasification for the fast gasifying biomass—sunflower seed shell. This does not directly

explain the gasification reactivity difference between both species, but it suggests that the evolution of these properties was a consequence of another catalytic mechanism.

Characterization of the inorganic compounds present in the chars revealed that, in addition to the difference of elemental composition, there was a difference in the volatility of K that was released for sunflower seed shells, but not for rice husks. Other differences concerned their form and location in the chars. Sunflower seed shell chars—that gasify faster—contained K and sometimes Ca directly into its carbonaceous matrix which was not the case for rice husk chars. In addition, some compounds such as KCl were present as small crystallites at the surface of the matrix for sunflower seed shell chars.

## 4. Conclusions

This study investigated the relative influence of the inorganic content compared to that of the physical properties of the biomass-derived chars on the gasification kinetics. In order to reach this goal, both organic and inorganic fractions of the chars obtained by pyrolysis and gasification were deeply characterized.

The analyses were performed on two types of biomass presenting significantly different gasification reactivities: rice husks that gasify slowly and sunflower seed shells that gasify faster. The aim was to determine the main parameter explaining this difference in terms of reactivity.

The results showed that the physico-chemical properties of the carbon matrix do not have a major influence on the gasification kinetics. On the opposite, the inorganic composition seems to be the parameter related to such reactivity differences of the two types of biomass. Moreover, the inorganics fraction also seemed to affect the physico-chemical characteristics of the produced chars, namely the microporosity and the amount of surface functions.

A more detailed identification and quantification of the various inorganic compounds will allow to explain their specific influence on the gasification kinetics and their mechanisms of action.

## Acknowledgement

The authors would like to acknowledge Maguelone Grateau for her help in producing the chars in the pyrolysis furnace.

The authors would also like to acknowledge Laurent Van De Steene from CIRAD for the setup of the macro-thermogravimetric reactor at USTH.

The authors thank Stéphanie Pouget for her assistance with P-XRD analysis.

Raman and nitrogen adsorption measurements were performed on the technical platforms of IS2M. The authors are very grateful to Simon Gree and Cyril Vaultot for their contribution.

The authors also thank Joseph Dentzer, Bénédicte Réty and Adrian Beda for their contribution with TPD-MS analysis.

## Funding

This research was funded by the Agence de l'Environnement et de la Maîtrise de l'Energie.

## References

- Ahmed, I.I., and Gupta, A.K. (2011). Kinetics of woodchips char gasification with steam and carbon dioxide. *Appl. Energy* 88, 1613–1619.
- Arnold, R.A., and Hill, J.M. (2019). Catalysts for gasification: a review. *Sustain. Energy Fuels* 3, 656–672.
- Arriagada, R., García, R., Molina-Sabio, M., and Rodriguez-Reinoso, F. (1997). Effect of steam activation on the porosity and chemical nature of activated carbons from Eucalyptus globulus and peach stones. *Microporous Mater.* 8, 123–130.
- Bale, C.W., Chartrand, P., Degterov, S.A., Eriksson, G., Hack, K., Ben Mahfoud, R., Melançon, J., Pelton, A.D., and Petersen, S. (2002). FactSage thermochemical software and databases. *Calphad* 26, 189–228.
- Barrio, M., Gøbel, B., Rimes, H., Henriksen, U., Hustad, J.E., and Sørensen, L.H. (2001). Steam Gasification of Wood Char and the Effect of Hydrogen Inhibition on the Chemical Kinetics. In *Progress in Thermochemical Biomass Conversion*, A.V. Bridgwater, ed. (John Wiley & Sons, Ltd), pp. 32–46.
- Bouraoui, Z., Dupont, C., Jeguirim, M., Limousy, L., and Gadiou, R. (2016). CO<sub>2</sub> gasification of woody biomass chars: The influence of K and Si on char reactivity. *Comptes Rendus Chim.* 19, 457–465.
- Chabalala, V.P., Wagner, N., and Potgieter-Vermaak, S. (2011). Investigation into the evolution of char structure using Raman spectroscopy in conjunction with coal petrography; Part 1. *Fuel Process. Technol.* 92, 750–756.
- Di Blasi, C. (2009). Combustion and gasification rates of lignocellulosic chars. *Prog. Energy Combust. Sci.* 35, 121–140.
- Dirbeba, M.J., Brink, A., DeMartini, N., Lindberg, D., and Hupa, M. (2016). Sugarcane vinasse CO<sub>2</sub> gasification and release of ash-forming matters in CO<sub>2</sub> and N<sub>2</sub> atmospheres. *Bioresour. Technol.* 218, 606–614.

- Dupont, C., Nocquet, T., Da Costa, J.A., and Verne-Tournon, C. (2011). Kinetic modelling of steam gasification of various woody biomass chars: Influence of inorganic elements. *Bioresour. Technol.* *102*, 9743–9748.
- Dupont, C., Jacob, S., Marrakchy, K.O., Hognon, C., Gateau, M., Labalette, F., and Da Silva Perez, D. (2016). How inorganic elements of biomass influence char steam gasification kinetics. *Energy* *109*, 430–435.
- ENS Lyon (2019). Handbook of Minerals Raman Spectra.
- European Standards (2009). Solid biofuels - Determination of ash content (EN 14775).
- Figueiredo, J.L., Pereira, M.F.R., Freitas, M.M.A., and Órfão, J.J.M. (1999). Modification of the surface chemistry of activated carbons. *Carbon* *37*, 1379–1389.
- Ganesh, A., Dutt Grover, P., and Iyer, P.V.R. (1992). Combustion and gasification characteristics of rice husk. *Fuel* *71*, 889–894.
- Guerrero, M., Ruiz, M.P., Millera, Á., Alzueta, M.U., and Bilbao, R. (2008). Oxidation Kinetics of Eucalyptus Chars Produced at Low and High Heating Rates. *Energy Fuels* *22*, 2084–2090.
- Guizani, C., Jeguirim, M., Gadiou, R., Escudero Sanz, F.J., and Salvador, S. (2016). Biomass char gasification by H<sub>2</sub>O, CO<sub>2</sub> and their mixture: Evolution of chemical, textural and structural properties of the chars. *Energy* *112*, 133–145.
- Guizani, C., Jeguirim, M., Valin, S., Limousy, L., and Salvador, S. (2017). Biomass Chars: The Effects of Pyrolysis Conditions on Their Morphology, Structure, Chemical Properties and Reactivity. *Energies* *10*, 796.
- Gupta, A., Thengane, S.K., and Mahajani, S. (2018). CO<sub>2</sub> gasification of char from lignocellulosic garden waste: Experimental and kinetic study. *Bioresour. Technol.* *263*, 180–191.
- Hack, K., Jantzen, T., Müller, M., Yazhenskikh, E., and Wu, G. (2012). A novel thermodynamic database for slag systems and refractory materials. In *Proceedings of the 5th International Congress on the Science and Technology of Steelmaking (Dresden, Germany)*.
- Hognon, C., Dupont, C., Gateau, M., and Delrue, F. (2014). Comparison of steam gasification reactivity of algal and lignocellulosic biomass: Influence of inorganic elements. *Bioresour. Technol.* *164*, 347–353.
- Huang, Y., Yin, X., Wu, C., Wang, C., Xie, J., Zhou, Z., Ma, L., and Li, H. (2009). Effects of metal catalysts on CO<sub>2</sub> gasification reactivity of biomass char. *Biotechnol. Adv.* *27*, 568–572.
- International Organization for Standardization (2015). Solid biofuels - Determination of major elements - Al, Ca, Fe, Mg, P, K, Si, Na and Ti (ISO 16967:2015).
- Kersten, S.R.A., Palz, W.D., Spitzer, J.D., Prins, W., Drift, A. van der, Maniatis, K.D., Kwant, K.D., Helm, P.D., and Grassi, A.D. (2002). Interpretation of biomass gasification by 'Quasi'-Equilibrium models. (*Sustainable Process Technology*), pp. 772–776.
- Kilpinen, P., Hupa, M., and Leppälähti, J. (1991). Nitrogen Chemistry at Gasification - A Thermodynamic Analysis (Åbo Akademi University).

- Krishnarao, R.V., Subrahmanyam, J., and Jagadish Kumar, T. (2001). Studies on the formation of black particles in rice husk silica ash. *J. Eur. Ceram. Soc.* *21*, 99–104.
- Lane, D.J., van Eyk, P.J., Ashman, P.J., Kwong, C.W., de Nys, R., Roberts, D.A., Cole, A.J., and Lewis, D.M. (2015). Release of Cl, S, P, K, and Na during Thermal Conversion of Algal Biomass. *Energy Fuels* *29*, 2542–2554.
- Link, S., Arvelakis, S., Hupa, M., Yrjas, P., Külaots, I., and Paist, A. (2010). Reactivity of the Biomass Chars Originating from Reed, Douglas Fir, and Pine. *Energy Fuels* *24*, 6533–6539.
- Liu, X., Zheng, Y., Liu, Z., Ding, H., Huang, X., and Zheng, C. (2015). Study on the evolution of the char structure during hydrogasification process using Raman spectroscopy. *Fuel* *157*, 97–106.
- Marquez-Montesinos, F., Cordero, T., Rodríguez-Mirasol, J., and Rodríguez, J.J. (2002). CO<sub>2</sub> and steam gasification of a grapefruit skin char. *Fuel* *81*, 423–429.
- Nguyen, H.N., Steene, L. van de, Le, T.T.H., Le, D.D., and Ha-Duong, M. (2018). Rice Husk Gasification: from Industry to Laboratory. *IOP Conf. Ser. Earth Environ. Sci.* *159*.
- Park, B.-D., Wi, S.G., Lee, K.H., Singh, A.P., Yoon, T.-H., and Kim, Y.S. (2003). Characterization of anatomical features and silica distribution in rice husk using microscopic and micro-analytical techniques. *Biomass Bioenergy* *25*, 319–327.
- Rodríguez-Reinoso, F., Molina-Sabio, M., and González, M.T. (1995). The use of steam and CO<sub>2</sub> as activating agents in the preparation of activated carbons. *Carbon* *33*, 15–23.
- Ryu, S.-E., Kim, T.-N., and Kang, T.-K. (1997). Pulverization of rice husks and the changes of husk densities. *J. Mater. Sci.* *32*, 6639–6643.
- Saavedra Rios, C. del M., Simone, V., Simonin, L., Martinet, S., and Dupont, C. (2018). Biochars from various biomass types as precursors for hard carbon anodes in sodium-ion batteries. *Biomass Bioenergy* *117*, 32–37.
- Sadezky, A., Muckenhuber, H., Grothe, H., Niessner, R., and Pöschl, U. (2005). Raman microspectroscopy of soot and related carbonaceous materials: Spectral analysis and structural information. *Carbon* *43*, 1731–1742.
- Septien, S., Escudero Sanz, F.J., Salvador, S., and Valin, S. (2018). The effect of pyrolysis heating rate on the steam gasification reactivity of char from woodchips. *Energy* *142*, 68–78.
- Sheng, C. (2007). Char structure characterised by Raman spectroscopy and its correlations with combustion reactivity. *Fuel* *86*, 2316–2324.
- Tascón, J.M. (2012). *Novel Carbon Adsorbents* (Elsevier).
- Thommes, M., Kaneko, K., Neimark, A.V., Olivier, J.P., Rodríguez-Reinoso, F., Rouquerol, J., and Sing, K.S.W. (2015). Physisorption of gases, with special reference to the evaluation of surface area and pore size distribution (IUPAC Technical Report). *Pure Appl. Chem.* *87*, 1051–1069.
- Vassilev, S.V., Baxter, D., Andersen, L.K., Vassileva, C.G., and Morgan, T.J. (2012). An overview of the organic and inorganic phase composition of biomass. *Fuel* *94*, 1–33.

Wang, Q., Zhang, R., Luo, Z., Fang, M., and Cen, K. (2016). Effects of Pyrolysis Atmosphere and Temperature on Coal Char Characteristics and Gasification Reactivity. *Energy Technol.* 4, 543–550.

Yip, K., Tian, F., Hayashi, J., and Wu, H. (2010). Effect of Alkali and Alkaline Earth Metallic Species on Biochar Reactivity and Syngas Compositions during Steam Gasification. *Energy Fuels* 24, 173–181.

Zahara, Z.F., Kudo, S., Daniyanto, Ashik, U.P.M., Norinaga, K., Budiman, A., and Hayashi, J. (2018). CO<sub>2</sub> Gasification of Sugar Cane Bagasse: Quantitative Understanding of Kinetics and Catalytic Roles of Inherent Metallic Species. *Energy Fuels* 32, 4255–4268.

Zhang, Y., Ashizawa, M., Kajitani, S., and Miura, K. (2008). Proposal of a semi-empirical kinetic model to reconcile with gasification reactivity profiles of biomass chars. *Fuel* 87, 475–481.

Zhao, Y., Feng, D., Zhang, Y., Huang, Y., and Sun, S. (2016). Effect of pyrolysis temperature on char structure and chemical speciation of alkali and alkaline earth metallic species in biochar. *Fuel Process. Technol.* 141, 54–60.